Journal of Holography Applications in Physics
Volume 5, Special Issue, Summer 2025, 1-82

DOI: 10.22128/jhap.2025.004.0026

Journal of Holography Applications in Physics

Conference Proceedings

4th International Conference on Holography and its Applications (ICHA4 2025)

18-19, September 2025

Baku, Azerbaijan

Committee of the ICHA4 2025
Khazar University
Tel: (+994 12) 421 10 93
Email: holography@du.ac.ir

Conference website: https://holography2025.du.ac.ir

Conference Proceedings of 4th International Conference on Holography and its Applications (ICHA4, 2025)

Edited by Dr. Hoda Farahani

Online ISSN: 2783-3518
Print ISSN: 2783-4778

ISBN : 978-622-5209-52-7

DOI: 10.22128/jhap.2025.004.0026

Published by Journal of Holography Applications in Physics (JHAP), Damghan University Press.
Tel: +98-23-35220236
Fax: +98-23-35220236

Hosting:
Khazar University, Baku, Azerbaijan

Organized By:
School of Physics, Damghan University, Damghan, Iran

Academic Partner:
Canadian Quantum Research Center (CQRC)

ICHA4 2025 Executive Committee

Dr. Hoda Farahani (Chief Executive Officer) *School of Physics, Damghan University, Iran*
Prof. Lawrence Krauss (Executive Committee member) *The Origins Project Foundation, USA*
Prof. Shahin Mammadov (Executive Committee member**)** *Khazar University, Azerbaijan*
Prof. Farida Tatardar (Executive Committee member**)** *Khazar University, Azerbaijan*
Prof. Behnam Pourhassan (Executive Committee member**)** *School of Physics, Damghan University, Iran*
Prof. Emil Akhmedov (Executive Committee member**)** *Khazar University, Azerbaijan*
Prof. Motoi Tachibana (Executive Committee member**)** *Khazar University, Azerbaijan*
Mr. Salman Sajad Wani (Executive Committee member**)** *Hamad Bin Khalifa University, Doha, Qatar*
Dr. Mehdi Shokri (Executive Committee member**)** *Canadian Quantum Research Center, Canada*
Dr. Nosratollah Jafari (Executive Committee member**)** *Khazar University, Azerbaijan*
Dr. Babak Khanbabaei (Executive Committee member**)** *School of Physics, Damghan University, Iran*
Morteza Tavakoli (Responsible for DU conferences) *Damghan University, Iran*

ICHA4 2025 Session Chairs

Prof. İzzet Sakallı *Eastern Mediterranean University, North Cyprus, Turkey*
Prof. Orhan Donmez *American University of the Middle East, Kuwait*
Prof. Shahin Mammadov, *Khazar University, Azerbaijan*
Prof. Behnam Pourhassan *School of Physics, Damghan University, Damghan, Iran*

ICHA4 2025 Scientific Committee

Prof. Behnam Pourhassan	(Conference Chair) *School of Physics, Damghan University, Iran*
Prof. Leonard Susskind	*Stanford Institute for Theoretical Physics, Stanford, USA*
Prof. Lawrence Krauss	*The Origins Project Foundation, USA*
Prof. Salvatore Capozziello	*Napoli University, Italy*
Prof. Robert Mann	*University of Waterloo, Canada*
Prof. Emmanuel Saridakis	*National Observatory of Athens, Greece*
Prof. Shahin Sheikh-Jabbari	*IPM, Iran*
Prof. Stefano Bellucci	*INFN, Laboratori Nazionali di Frascati, Roma, Italy*
Prof. Xiaoping Shi	*Uiversity of British Columbia, Okanagan, Canada*
Prof. Ligang Wang	*Zhejiang University, China*
Prof. Kourosh Nozari	*University of Mazandaran, Iran*
Prof. Bayram Tekin	*Middle East Technical University, Turkey*
Prof. Jafar Sadeghi	*University of Mazandaran, Babolsar, Iran*
Prof. İzzet Sakallı	*Eastern Mediterranean University, North Cyprus, Turkey*
Prof. Emre Onur Kahya	*Istanbul Technical University, Turkey*
Prof. Celia Escamilla-Rivera	*Instituto de Ciencias Nucleares, Mexico*
Prof. Latham Boyle	*Perimeter Institute for Theoretical Physics, Canada*
Prof. Sayyed Ali Asghar Alavi	*Hakim Sabzevari University, Iran*
Prof. Mario C. Rocca	*Consejo Nac. de Investigaciones Científicas y Técnicasdisabled, Argentina*
Prof. Abolfazl Mirjalili	*Yazd University, Iran*
Prof. Kazem Bitaghsir Fadafan	*Shahrood University of Technology, Iran*
Dr. Hoda Farahani	*School of Physics, Damghan University, Iran*
Dr. Haidar Sheikhahmadi	*IPM, Iran and North-West University, South Africa*
Dr. Shahab Shahidi	*School of Physics, Damghan University, Iran*

ICHA4 2024 Editorial Board

Message From the Damghan University President

In the name of God

Hello and welcome to the participants and speakers of the 4th International Conference on Holography and its Applications.

With the aim of expanding and promoting science and also promoting of scientific and industrial progress, Damghan University has always sought to increase international interactions and has supported all kinds of effective activities in this direction. For this reason, in recent years, Damghan University has organized several international conferences in the fields of physics, mathematics, biology and industrial engineering.

The first conference with the aim of gathering research and researchers in the field of holography in one collection was held on 2022, the second one on 2023, and the third one on 2024.

We are so happy to witness this great event again after about 1 year and we hope to have a successful conference like the previous ones. In this conference, like the previous ones, brilliant physicists from Iran and around the world were present as speakers and participants. Today, this conference is supported by many associations and scientific institutions and domestic and foreign universities.

Although this conference is also held virtually due to health issues, but there is an in-person part organized by Khazar university.

In the end, I hope that attending this conference will be beneficial for all the participants, and I would also like to thank and appreciate the keynote speakers of this conference who will give speeches in this conference despite being very busy.

Prof. Reza Pourgholi

Damghan University President

Message From the Conference Chair ICHA4 2025

Hello, I am Behnam Pourhassan, the conference chairman. Nice to see you here for the 4th time. Welcome all to the fourth International Conference on Holography and its Applications.

Conference Organizers

Fourth International Conference on Holography and its Applications, organized by Damghan University, the Canadian Quantum Research Center, and the Khazar University.

Many thanks Prof. Shahin Mamedov and Khazar University for hosting this conference.

We are excited to share that the conference proceedings and selected papers will be published by the Journal of Holography Applications in Physics (JHAP).

JHAP is already indexed by Scopus as promised in last year.

In this year we awarded the fourth JHAP Prize. Congratulations Dr. Prabir Rudra, winner of the fourth JHAP Prize. There is also another prize for the next issue.

Damghan University consider also a big prize: 2025 Prizes for Letters on Holography

Winners will be introduced tomorrow in closing session.

- The conference program is available on the conference website:

https://holography2025.du.ac.ir/en/

- This conference has two parts: Online and In-person talks. I hope to have fully in-person conference in future.
- Our next goal is indexing the conference in Scopus. We have already obtained ISBN for the previous proceedings and we will also obtain an ISSN for the conference.

This conference is a joint activity between the Damghan University and the Canadian Quantum Research Center So, at the first, we invite Scott Jacobsen administrative director of CQRC to give a talk, then we attend seminar which will begin with the Prof. Salvatore Capozziello.

Prof. B. Pourhassan,

Conference Chair ICHA4 2025,
Damghan University,
Iran

Message From the Academic Partner Administrative ICHA4 2025

Please see the following links.

Scott Jacobsen Message: https://www.youtube.com/watch?v=seQ5RaJXwFU

Page No

Table of Contents

Part One

Keynote Speakers

Introduction to black hole thermodynamics

Edward Witten

School of Natural Sciences, Institute for Advanced Study, Princeton, NJ 08540, USA

Abstract: I will explain the basics of black hole thermodynamics, which combines gravity, quantum mechanics, and thermodynamics in s fascinating way.

References

[1] Edward Witten, Eur.Phys.J.Plus 140 (5) 430 (2025)

[2] S. W. Hawking, Commun. Math. Phys. 43, 199-220 (1975)

[3] D. Christodoulou, Phys. Rev. Lett. 25, 1596 (1970)

Talk link: https://youtu.be/E5AcqO2rTfY

Friday 19th September 2025

Observers in de Sitter Space

Leonard Susskind

Stanford Institute for Theoretical Physics, USA

Department of Physics, Stanford University, Stanford, USA

Abstract: I'll discuss the importance of physical observers (or quantum reference frames) in a holographic theory of de Sitter Space.

References

[1] Leonard Susskind, Journal of Holography Applications in Physics 5 (2) 1-9 (2025)

[2] L. Susskind, Journal of Holography Applications in Physics 3 (1) 1-30 (2023)

[3] H. Lin and L. Susskind, [arXiv:2206.01083 [hep-th]].

Talk link: https://youtu.be/NSSgoQyd12E

Friday 19th September 2025

Doubly Holographic Quantum Black Holes

Robert B. Mann

University of Waterloo, Waterloo, Canada

Abstract: Quantum black holes are exact solutions to a semi-classical gravitational theory that incorporates all orders of quantum field backreaction on spacetime. These black holes have a doubly holographic thermodynamic description relating bulk to brane and brane to boundary. If uncharged, they exhibit re-entrant phase transitions and critical exponents that differ from standard mean field theory. The presence of charge and rotation eliminates these phenomena, with the critical exponents the same as in mean-field theory.

An energy scale (or mass gap) M_{gap} can be computed to identify regimes where quantum fluctuations of spacetime geometry are expected to become significant. Their gyromagnetic ratio is a function of the backreaction, and approaches a constant in the limit backreaction effects are large. This class of black holes respects quantum versions of the Penrose and reverse isoperimetric inequalities. Taken as a whole, such black holes provide an interesting new test bed for confronting gravitation with quantum physics.

References

[1] Robert B. Mann, Journal of Holography Applications in Physics 4 (1) 1-26 (2024).

[2] D. Kastor, S. Ray, and J. Traschen,

Class. Quant. Grav. 26, 195011 (2009).

[3] B. P. Dolan, Class. Quant. Grav. 28, 235017 (2011).

[4] B. P. Dolan, Class. Quant. Grav. 28, 125020 (2011).

Talk link: https://youtu.be/dGg0AL2EZEE

Thursday 18th September 2025

Avoiding singularities in Lorentzian-Euclidean black holes: The role of atemporality

Salvatore Capozziello

Napoli University, Italy

Abstract: We investigate a Schwarzschild metric exhibiting a signature change across the event horizon, which gives rise to what we term a Lorentzian-Euclidean black hole. The resulting geometry is regularized employing the Hadamard partie finie technique, which allows us to prove that the metric represents a solution of vacuum Einstein equations. In this framework, we introduce the concept of atemporality as the dynamical mechanism responsible for the transition from a regime with a real-valued time variable to a new one featuring an imaginary time. We show that this mechanism prevents the occurrence of the singularity and discuss that, thanks to the regularized Kretschmann invariant, the atemporality can be considered as a characteristic feature of this black hole.

References

[1] Salvatore Capozziello, Silvia De Bianchi, Emmanuele Battista, Phys.Rev.D 109, 10, 104060 (2024).

[2] T. Dereli, M. Onder, and R. W. Tucker, Class. Quant. Grav. 10, 1425 (1993).

[3] J. B. Hartle and S. W. Hawking, Phys. Rev. D 28, 2960 (1983).

[4] S. W. Hawking, R. Laflamme, and G. W. Lyons, Phys. Rev. D 47, 5342 (1993).

[5] A. D. Linde, Lett. Nuovo Cim. 39, 401 (1984).

[6] A. Vilenkin, Phys. Lett. B 117, 25 (1982).

[7] A. Vilenkin, Phys. Rev. D 58, 067301 (1998).

Talk link: https://youtu.be/dGg0AL2EZEE

Thursday 18th September 2025

Part Two

Invited Talks

Ghost Condensate Dark Energy with Sextic Dispersion Relation in de Sitter Spacetime

Amjad Ashoorioon

School of Physics, The Institute for Research in Fundamental Sciences (IPM), Tehran, Iran

Abstract: We study the ghost condensate (GC) with a sixth-order dispersion relation $\omega^2 \sim k^6$, within the effective field theory framework of dark energy. Unlike the GC with a quartic dispersion relation, we find that in the sextic case, the correction to the Newtonian potential depends explicitly on the space and time variations of the matter density. At very late times, the resulting modification exhibits oscillatory behavior at distances of order M_{Pl}/M^2, at the timescale ${M^4}/{M_{Pl}}^3$, where M^2 corresponds to the scale of the ghost condensate. We analyze scalar and tensor perturbations in both FLRW and de Sitter backgrounds, and show that the gravitational potential receives non-trivial, scale-dependent modifications arising from the inclusion of higher-derivative operators in the effective action. In the FLRW background, we compute the effective gravitational constant G_{eff} and the gravitational slip parameter, γ in the sub-horizon limit $k/a \gg H$, revealing their explicit dependence on spatial scales. Additionally, we demonstrate that the speed of gravitational waves becomes frequency dependent, with significant deviations from luminal propagation arising at momenta near $M_{Pl}/\sqrt{|\sigma_1|}$, where σ_1 is the coefficient of the operator $\gamma^{ij}\nabla_i K_{lr}\nabla_j K^{lr}$in the unitary gauge action.

References

[1] A. G. Riess, et al., Observational evidence from supernovae for an accelerating universe and a cosmological constant, Astron. J. 116 (1998) 1009–1038. arXiv:astro-ph/9805201, doi:10.1086/300499.

[2] S. Perlmutter, et al., Measurements of Ω and Λ from 42 high redshift supernovae, Astrophys. J. 517 (1999) 565–586. arXiv:astro-ph/9812133, doi:10.1086/307221.

[3] N. Aghanim, et al., Planck 2018 results. I. Overview and the cosmological legacy of Planck, Astron. Astrophys. 641 (2020) A1. arXiv:1807.06205, doi:10.1051/0004-6361/201833880.

[4] A. G. Riess, et al., A Comprehensive Measurement of the Local Value of the Hubble Constant with 1 km/s/Mpc Uncertainty from the Hubble Space Telescope and the SH0ES Team, Astrophys. J. Lett. 934 (1) (2022) L7. arXiv:2112.04510, doi:10.3847/2041-8213/ ac5c5b

Talk link: https://youtu.be/LloLZiKqR_Q

Friday 19th September 2025

Generation and Applications of Structured Light Beams with Various Symmetries

Saifollah Rasouli

Institute for Advanced Studies in Basic Sciences, Iran

Abstract: This talk presents the generation of diverse structured light beams through diffraction of plane waves by diffractive elements with both axial and non-axial symmetries. The resulting beams include symmetric, asymmetric, and elliptical radial carpet beams, as well as combined Bessel-like beams in both symmetric and elliptical forms. Symmetric radial carpet beams are produced by diffraction of plane waves from radial phase and amplitude gratings with sinusoidal and binary profiles, while fractional radial carpet beams are generated using gratings with a fractional number of spokes. Elliptical radial carpet beams emerge when plane waves diffract from the grating in uniaxial crystals. Furthermore, combining radial phase and amplitude structures yields combined Bessel-like beams, and applying elliptical modulation to the azimuthal periodicity of these structures produces elliptical combined Bessel-like beams. Another type, galaxy-like beams, exhibit multiple intensity spots that rotate around the optical axis during propagation, generated by plane-wave diffraction from spiral–radial amplitude structures.

All these beams exhibit key features such as acceleration, self-healing, low divergence, and self-amplification within their patterned core regions. These properties make them robust against atmospheric turbulence and suitable for free-space optical communications in turbulent media. Their two-dimensional (2D) array-like transverse intensity distribution in polar coordinates also enables multi-particle trapping, while variations in the transverse intensity patterns—arising from different spoke numbers in the generating gratings—provide opportunities for spatial-mode-based information transfer. Finally, the generation and multiplication of structured beams in Cartesian coordinates are discussed in both near- and far-field regimes. In the near field, forked and 2D amplitude gratings are employed in

conjunction with the Talbot effect, while in the far field, forked gratings and almost-periodic amplitude structures are used.

References

[1] A. Forbes, M. de Oliveira, and M. R. Dennis, “Structured light,” Nature Photonics 15, 253–262 (2021).

[2] Y. Shen and C. Rosales-Guzmán, “Nonseparable states of light: From quantum to classical,” Laser & Photonics Reviews 16, 2100533 (2022).

Talk link: https://youtu.be/uqW5avMcUek

Friday 19th September 2025

Entanglement islands and Page curve in the framework of Horndeski gravity

Fabiano F. Santos

Centro de Ciências Exatas, Naturais e Tecnológicas, UEMASUL, 65901-480, Imperatriz, MA, Brazil

Departamento de Física, Universidade Federal do Maranhão, São Luís, 65080-805, Brazil

Abstract: We study entanglement islands and the Page curve in Horndeski gravity on a Karch-Randall braneworld. Analyzing the holographic boundary conformal field theory, we find that Horndeski parameters significantly modify the Page curve due to the geometry induced by the Horndeski scalar field. Notably, the geometry far from the AdS limit plays a key role, highlighting how Horndeski gravity impacts quantum information distribution. Additionally, holographic consistency offers a way to constrain Horndeski gravity, providing a tool to test modified gravity theories.

References

[1] S. W. Hawking, Particle Creation by Black Holes,' Commun. Math. Phys. 43, 199-220 (1975) [erratum: Commun. Math. Phys. 46, 206 (1976)].

[2] S. W. Hawking, Breakdown of Predictability in Gravitational Collapse, Phys. Rev. D 14, 2460-2473 (1976).

[3] L. Susskind, Computational Complexity and Black Hole Horizons, Fortsch. Phys. 64, 24-43 (2016) [arXiv:1402.5674 [hep-th]]; (Addendum) ibid. 44-48 [arXiv:1403.5695 [hep-th]].

Talk link: https://youtu.be/w4T2LjO5FVc

Friday 19th September 2025

Renormalization of QFT in USR inflation: Recent developments

Haidar SheikhAhmadi

School of Astronomy, Institute for Research in Fundamental Sciences (IPM), Tehran, Iran

Center for Space Research, North-West University, Potchefstroom, South Africa

Abstract: In this talk, I will review recent contradictions in QFT contributions to Ultra-Slow-Roll inflation models. After renormalizing the infinities and applying effective field theory, I will show that the 1-loop corrections persist without cancellation.

References

[1] Haidar Sheikhahmadi, Amin Nassiri-Rad, "Renormalized one-Loop Corrections in Power Spectrum in USR Inflation", arXiv:2411.18525 [astro-ph.CO]

[2] Amin Nassiri-Rad, Haidar Sheikhahmadi, Hassan Firouzjahi, "Stochastic Inflation with Interacting Noises", arXiv:2508.09946 [astro-ph.CO]

Talk link: https://youtu.be/wS_Ea0J_wjo

Friday 19th September 2025

Dunkl Black Holes with Phantom Global Monopoles: Geodesic Analysis and Thermodynamic Properties

İzzet Sakallı

Physics Department, Eastern Mediterranean University, Famagusta 99628, North Cyprus via Mersin 10, Turkey

Abstract: We present a comprehensive analysis of static spherically symmetric black hole solutions within the framework of Dunkl geometry, incorporating the effects of both ordinary and phantom global monopoles. This work extends classical black hole physics by introducing topological defects and modified symmetry structures via Dunkl operators, which exhibit exotic repulsive gravitational effects in the presence of phantom global monopoles.

Our investigation focuses on null geodesics with particular emphasis on photon dynamics, trajectory behavior, and circular photon orbits near these modified black holes. We analyze the stability properties through effective potential analysis and examine how the Dunkl parameter and phantom global monopoles significantly alter light propagation characteristics compared to classical solutions such as the Schwarzschild black hole.

The thermodynamic analysis reveals substantial deviations in key quantities including Hawking temperature, entropy, Gibbs free energy, and specific heat. We demonstrate how these modifications provide valuable insights into thermal behavior and phase transitions in the context of Dunkl geometry. Additionally, we investigate the formation and characteristics of black hole shadows in this spacetime, showing that the inclusion of Dunkl symmetry and phantom global monopoles leads to profound modifications in both the physical and geometric properties of the black hole.

Our findings highlight the significant role of the Dunkl parameter in modifying spacetime geometry and suggest potential observational signatures that could distinguish these exotic black holes from their classical counterparts. This research contributes to the growing field of modified gravity theories and their implications for black hole physics and cosmology.

References

[1] A. Al-Badawi, F. Ahmed and İzzet Sakallı, Eur. Phys. J. C 85, no.6, 660 (2025).

Talk link: https://youtu.be/xMYQaiv-HhA

Thursday 18th September 2025

The modular Dirac equation and cryptography

Christina Rugina

Canadian Quantum Research Center, 204-3002 32 Ave, Vernon, BC V1T 2L7, Canada

Department of Physics, University of Bucharest, Bucharest, Romania

Abstract: The modular flow on the boundary of an AdS_2 spacetime ensures that the entanglement wedge and the causal wedge coincide. We previously proposed that we can effectively 'see' at the center of the bulk with the help of the modular Dirac equation, so we now go ahead and predict the fact that the entire bulk is actually computable by a quantum computer that can 'see' behind the horizon if a proper cryptographic key is available and that such a key is linked to the existence of the AdS_2 SL(2) generators found by Lin, Maldacena and Zhao in 2019.

References

[1] S. D. Mathur, ”The information paradox: A pedagogical introduction”, Class. Quant. Grav. 26, 224001 (2009), arXiv:0909.1038.

[2] L. Susskind, L. Thorlacius, J. Uglum, ”The stretched horizon and black hole complementarity”, Phys.Rev.D 48, 3743 (1993), arxiv: hep-th/9306069.

[3] J. Maldacena, L. Susskind, ”Cool horizons for entangled black holes”, Fortsch. Phys. 61, 781 (2013), arxiv: 1306.0533.

[4] S. W. Hawking, M. J. Perry, A. Strominger, ”Soft Hair on Black Holes”, Phys. Rev. Lett. 116, 231301 (2016), arXiv:1601.00921.

[5] A. Sen, ”Extremal black holes and elementary string states”, Mod. Phys. Lett. A 10, 2081 (1995), hep-th/9504147.

Talk link: https://youtu.be/QJ-f5H9kHHI

Friday 19th September 2025

Part Three

Poster presentations

Virtual

Proceedings of the 4th International Conference on Holography and its Applications

18 to 19 September, 2025, Khazar University, Baku, Azerbaijan. ICHA4(2025)301

Full paper - Poster

Investigation of Rotating Magnetic Brane Solutions of Quasitopological Gravity in The Presence of Exponential Nonlinear Field

Alireza Alizadeh[1], Saheb Soroushfar[2].
[1] Department of Physics, Colleg of sciences, Yasuj University, 75918-74934, Iran.
Email: Alirezaalizadeh02@gmail.com
[2] Department of Physics, Colleg of sciences, Yasuj University, 75918-74934, Iran.
Email: Soroush@yu.ac.ir

Abstract. In this paper, we obtain Rotating magnetic brane solutions of quasi-topological gravity in the presence of exponential nonlinear electrodynamic with one or more rotation parameters. For the rotating brane, the brane has a net electric charge, when one or more rotation is non zero. These solutions are horizonless and have no curvature, but there is a conic singularity with a deficit angle δ. Finally, we analyze the behaviors of the solutions function for the various parameters.

1 Introduction

Since, many systems in nature that include equations of gravitational systems are inherently nonlinear, in recent years, there has been a great deal of motivation to conduct studies related to quasi-topological gravity and nonlinear electrodynamics. We can name exponential [1] as the type of nonlinear electrodynamics theory, which are defined as

$$L_{exp}(F) = 4\beta^2\left(exp\left(\frac{-F^2}{4\beta^2}\right) - 1\right) \quad (1)$$

$$F^2 = F_{\mu\nu}F^{\mu\nu} \quad (2)$$

β is the nonlinear parameter with dimension of mass and $F = F_{\mu\nu}F^{\mu\nu}$, where $F_{\mu\nu}$ is the electromagnetic field tensor that is defined as $F_{\mu\nu} = \partial_\mu A_\nu - \partial_\nu A_\mu$ andA_μ is the vector potential. On the other hand, this Lagrangian reduce to the linear Maxwell Lagrangian as $\beta \to \infty$. Like the Born - Infeld theory, exponential nonlinear electrodynamics theory eliminates the infinity of the electric field [2, 3], while the exponential form is unable to do, but this theory causes a weaker singularity than the one in Einstein-Maxwell theory [4]. The exponential form cannot cancel this infinity, but it causes a weaker singularity than the one in Einstein-Maxwell theory [5]. Also, magnetic branes are attractive because their solutions are horizonless and have a conical geometry. Now, we have a decision to take a further step and study the solutions magnetic branes with exponential nonlinear electrodynamic in quartic quasitopological gravity. In this paper, we begin with the metric of a horizonless spacetime and an action including nonlinear electrodynamic and quartic quasitopological theories. Then, we obtain equations and solutions and also, we investigate physical structure and behavior of the obtained solutions. At last, we write a brief result of the obtained data from this magnetic brane.

2 Rotating Metric and Solutions

We want to abtain the solutions with no horizons. Therefore, we start with a metric with characteristics $\left(g_{\rho\rho}\right)^{-1} \propto g_{\phi\phi}$ and $g_{tt} \propto -\rho^2$ instead of $\left(g_{\rho\rho}\right)^{-1} \propto g_{tt}$ and $g_{\phi\phi} \propto -\rho^2$. So, we will work with the following rotating metric

$$ds^2 = \left[-\frac{\rho^2}{l^2}\Xi^2 + g(\rho)\Xi^2 - g(\rho)\right]dt^2 + 2\left[\frac{\rho^2}{l}\Xi\sqrt{\Xi^2-1} - lg(\rho)\Xi\sqrt{\Xi^2-1}\right]dtd\phi + \frac{1}{f(\rho)}d\rho^2 + [-\rho^2\Xi^2 + \rho^2 + l^2 g(\rho)\Xi^2]d\phi^2 + \frac{\rho^2}{l^2}dX^2 \quad (3)$$

where l is a scale factor that is related to the cosmological constant Λ. $dX^2 = \sum_{i=1}^{n-2}$ is a $(n-2)$-dimensional hypersurface with the form of a Euclidean metric in volume V_{n-2}. ρ and ϕ are, respectively, the radial and angular coordinates at which ϕ is dimensionless and has the range$0 \le \phi \le 2\pi$. The action of quartic quasi-topological in $(n+1)$-dimensions in the presence of nonlinear electrodynamic theory is

$$I_G = \int d^{n+1}\sqrt{-g}\left[-2\Lambda + \mathcal{L}_1 + \hat{\lambda}\mathcal{L}_2 + \hat{\mu}\mathcal{L}_3 + \hat{c}\mathcal{L}_4 + L(F)\right] \quad (4)$$

Where g is the determinant of the metric (3) and $\Lambda = -\frac{n(n-1)}{2l^2}$. Just the Einstein-Hilbert lagrangian, second order Lovelock or Gauss-Bonnet lagrangian, cubic and quartic quasi topological Lagrangians are respectively defined as

$$\mathcal{L}_1 = \mathrm{R} \quad (5)$$

$$\mathcal{L}_2 = R_{abcd}R^{abcd} - 4R_{ab}R^{ab} + R^2 \quad (6)$$

$$\mathcal{L}_3 = R_{ab}^{cd}R_{cd}^{ef}R_{ef}^{ab} + \frac{1}{(2n-1)(n-3)}\frac{3(3n-5)}{8}R_{abcd}R^{abcd}R - 3(n-1)R_{abcd}R_e^{abc}R^{de} + 3(n+1)R_{abcd}R^{ac}R^{bd} + 6(n-1)R_a^bR_b^cR_c^a - \frac{3(3n-1)}{2}R_a^bR_b^aR + \frac{3(n+1)}{8}R^3 \quad (7)$$

$$\mathcal{L}_4 = c_1R_{abcd}R^{cdef}R_{ef}^{hg}R_{hg}^{ab} + c_2R_{abcd}R^{abcd}R_{ef}R^{ef} + c_3RR_{ab}R^{ac}R_c^b + c_4(R_{abcd}R^{abcd})^2 + c_5R_{ab}R^{ac}R_{cd}R^{db} + c_6RR_{abcd}R^{ac}R^{db} + c_7R_{abcd}R^{ac}R^{be}R_e^d + c_8R_{abcd}R^{acef}R_e^bR_f^d + c_9R_{abcd}R^{ac}R_{ef}R^{bedf} + c_{10}R^4 + c_{11}R_{abcd}R^{abcd}R^2 + c_{12}R_{ab}R^{ab}R^2 + c_{13}R_{abcd}R^{cbef}R_{ef\ g}^cR^{dg} + c_{14}R_{abcd}R^{acef}R_{gehf}R^{gbhd} \quad (8)$$

where

$$\mathrm{c}_1 = -(\mathrm{n}-1)(\mathrm{n}^7 - 3\mathrm{n}^6 - 29\mathrm{n}^5 + 170\mathrm{n}^4 - 349\mathrm{n}^3 + 348\mathrm{n}^2 - 180\mathrm{n} + 36)$$

$$\mathrm{c}_2 = -4(\mathrm{n}-3)(2\mathrm{n}^6 - 20\mathrm{n}^5 + 65\mathrm{n}^4 - 81\mathrm{n}^3 + 13\mathrm{n}^2 + 45\mathrm{n} - 18)$$
$$\mathrm{c}_3 = -64(\mathrm{n}-1)(3\mathrm{n}^2 - 8\mathrm{n} + 3)(\mathrm{n}^2 - 3\mathrm{n} + 3)$$
$$\mathrm{c}_4 = -(\mathrm{n}^8 - 6\mathrm{n}^7 + 12\mathrm{n}^6 - 22\mathrm{n}^5 + 114\mathrm{n}^4 - 345\mathrm{n}^3 + 468\mathrm{n}^2 - 270\mathrm{n} + 54)$$
$$\mathrm{c}_5 = 16(\mathrm{n}-1)(10\mathrm{n}^4 - 51\mathrm{n}^3 + 93\mathrm{n}^2 - 72\mathrm{n} + 18)$$
$$\mathrm{c}_6 = 32(\mathrm{n}-1)^2(\mathrm{n}-3)^2(3\mathrm{n}^2 - 8\mathrm{n} + 3)$$
$$\mathrm{c}_7 = 64(\mathrm{n}-2)(\mathrm{n}-1)^2(4\mathrm{n}^3 - 18\mathrm{n}^2 + 27\mathrm{n} - 9)$$
$$\mathrm{c}_8 = -96(\mathrm{n}-1)(\mathrm{n}-2)(2\mathrm{n}^4 - 7\mathrm{n}^3 + 4\mathrm{n}^2 + 6\mathrm{n} - 3)$$
$$\mathrm{c}_9 = 16(\mathrm{n}-1)^3(2\mathrm{n}^4 - 26\mathrm{n}^3 + 93\mathrm{n}^2 - 117\mathrm{n} + 36)$$
$$\mathrm{c}_{10} = \mathrm{n}^5 - 31\mathrm{n}^4 + 168\mathrm{n}^3 - 360\mathrm{n}^2 + 330\mathrm{n} - 90$$
$$\mathrm{c}_{11} = 2(6\mathrm{n}^6 - 67\mathrm{n}^5 + 311\mathrm{n}^4 - 742\mathrm{n}^3 + 936\mathrm{n}^2 - 576\mathrm{n} + 126)$$
$$\mathrm{c}_{12} = 8(7\mathrm{n}^5 - 47\mathrm{n}^4 + 121\mathrm{n}^3 - 141\mathrm{n}^2 + 63\mathrm{n} - 9)$$
$$\mathrm{c}_{13} = 16\mathrm{n}(\mathrm{n}-1)(\mathrm{n}-2)(\mathrm{n}-3)(3\mathrm{n}^2 - 8\mathrm{n} + 3)$$
$$\mathrm{c}_{14} = 8(\mathrm{n}-1)(\mathrm{n}^7 - 4\mathrm{n}^6 - 15\mathrm{n}^5 + 122\mathrm{n}^4 - 287\mathrm{n}^3 + 297\mathrm{n}^2 - 126\mathrm{n} + 18) \quad (9)$$

$\hat{\lambda}$, $\hat{\mu}$ and $\hat{c}$ are respectively the parameters of Gauss-Bonnet, cubic and quartic quasi- topological Lagrangians. Actually, these parameters are arbitrary coupling constants, and rescaling is done to simplify the field equations. So, gives [6, 7]

$$\hat{\lambda} = \frac{\lambda l^2}{(n-2)(n-3)} \tag{10}$$

$$\hat{\mu} = \frac{7(2n-1)l^4\mu}{(n-2)(n-5)(3n^2-9n+4)} \tag{11}$$

$$\hat{c} = \frac{cl^6}{n(n-1)(n-3)(n-7)(n-2)^2(n^5-15n^4+72n^3-156n^2+150n-42)} \tag{12}$$

For the static magnetic brane, the vector potential has only one component A_ϕ, while for the rotating magnetic brane, add angular momentum to the spacetime. So, in this class, the vector potential includes two components A_ϕ and A_t. Therefore, the vector potential for the rotating solutions as

$$A_\mu = h(\rho)(\frac{\sqrt{\Xi^2-1}}{l}\delta_\mu^t - \Xi\delta_\mu^\phi) \tag{13}$$

Using the above relations in action (4) and integrating by parts, we can get the action

$$S = \frac{(n-1)}{16\pi l^2}\int d^n x \int d\rho N(\rho)\,[[\rho^n(1+\psi+\lambda\psi^2+\mu\psi^3+c\psi^4)]' + \frac{4\beta^2 l^2\rho^{n-1}}{n-1}\left[exp\left(-\frac{h'^2}{2\beta^2 l^2 N^2(\rho)}\right)-1\right]\Bigg] \tag{14}$$

where $g(\rho) = N(\rho)^2 f(\rho)$, $\psi(\rho) = -l^2\rho^{-2}f(\rho)$ and prime represents the first derivative with respect to ρ. Varying this action with respect to $\psi(\rho)$ yields

$$[1 + 2\lambda\psi(\rho) + 3\mu\psi^2(\rho) + 4c\psi^3(\rho)]N'(\rho) = 0 \tag{15}$$

The above equation shows that $N(\rho)$ must be a constant value, which we choose $N(\rho) = 1$. Varying the action (14) with respect to $N(\rho)$ and $h(\rho)$ and substituting $N(\rho)$=1 (or $g(\rho) = f(\rho)$) yields

$$[(n-1)\rho^n((1+\psi+\lambda\psi^2+\mu\psi^3+c\psi^4)]' + \rho^{n-1}\left(l^2\beta^2 + h'^2\right)exp\left(-\frac{h'^2}{2l^2\beta^2}\right) - 4l^2\beta^2\,\rho^{n-1} = 0$$

(16) $$\left(\rho^{n-1}h'\exp\left(-\frac{h'^2}{2l^2\beta^2}\right)\right)' = 0 \tag{17}$$

If we solve Eq. (17), we get the electromagnetic field

$$F_{\phi\rho} = \Xi h' = \Xi l\beta\sqrt{-Lw(-\eta)} \tag{18}$$

and

$$F_{t\rho} = \frac{\sqrt{\Xi^2-1}}{l\Xi}F_{\phi\rho} = \Xi h' = -l\beta\frac{\sqrt{\Xi^2-1}}{l}\sqrt{-Lw(-\eta)} \tag{19}$$

where $\eta = \frac{q^2 l^{2n-6}}{\beta^2\rho^{2n-2}}$ and q is the constant of integration. *Lw* is the Lambert function.

We get to the relation $F_{\phi\rho} = -\partial_\rho A_\phi$ and $F_{t\rho} = -\partial_\rho A_t$.

$$A_\phi = -\Xi\frac{n-1}{n-2}l\beta\left(\frac{l^{n-3}q}{\beta}\right)^{\frac{1}{n-1}}\left(-Lw(-\eta)\right)^{\frac{n-2}{2(n-1)}} \times \left\{2F_1\left(\left[\frac{n-2}{2(n-1)}\right],\left[\frac{3n-4}{2(n-1)}\right],-\frac{1}{2(n-1)}Lw(-\eta)\right)\right. \tag{20}$$

Using equation (18) in equation 16 leads to the relation

$$c\psi^4 + \mu\psi^3 + \lambda\psi^2 + \psi + k = 0 \tag{21}$$

where k is

$$k = 1 - \frac{M}{(n-1)\rho^n} + -\frac{4l^2\beta^2}{n(n-1)} - \frac{4(n-1)q\beta l^{n-1}}{n(n-2)\rho^n}\left(\frac{l^{n-3}q}{\beta}\right)^{\frac{1}{n-1}}\left(-Lw(-\eta)\right)^{\frac{n-2}{2(n-1)}} \times$$
$$2^{F_1}\left(\left[\frac{n-2}{2(n-1)}\right],\left[\frac{3n-4}{2(n-1)}\right],-\frac{1}{2(n-1)}Lw(-\eta)\right) + \frac{4\beta q l^{n-1}}{(n-1)\rho^{n-1}}\left(-Lw(-\eta)\right)^{\frac{1}{2}} \times \left[1+\frac{1}{n}(-Lw(-\eta))^{-1}\right] \quad (22)$$

and M is the integration constant and is related to the mass of this magnetic brane. In the above solution, we have used the following relation for the Lambert function:

$$Lw(x)e^{Lw(x)} = x \quad (23)$$

Finally, the solution $f(\rho)$ for Eq. (21) is obtained as

$$f(\rho) = -\frac{\rho^2}{l^2}\left(-\frac{\mu}{4c} + \frac{\pm_s W \mp_t \sqrt{-(3\alpha+2y\pm_s\frac{2\beta}{W})}}{2}\right) \quad (24)$$

In the above equation, two $\pm_s$ should both have the same sign, while the sign of $\mp_t$ is independent. It is noteworthy to say that in order to have the cubic quasi-topological or Gauss-Bonnet solutions we should replace $\mu = 0$ or $\lambda = 0$ in Eq. (21) and not find the solutions in the above relations because we get vague values [6,8,9].

3 Physical Properties of The Solutions

In this section, we aim to investigate the geometric and physical properties of the solutions like horizons, singularity, and behaviors of the function $f(\rho)$. As we know, to find the horizons of the obtained solutions, the condition $f(r_+) = 0$ should be satisfied where r_+ is the horizon. Suppose that r_+ is the largest real root of $f(\rho) = 0$, which leads to the function $f(\rho)$ being positive for $\rho > r_+$and negative for $\rho < r_+$. The range $0 < \rho < r_+$ is not acceptable as $g_{\rho\rho}$ cannot be negative (which occurs for $\rho < r_+$, because of the change of signature of the metric from $(n-1)+$ to $(n-2)+$. Therefore, we delete this unacceptable range $0 < \rho < r_+$, and so the function $f(\rho)$ is limited to the acceptable range $\rho > r_+$. For ease, we can use the suitable transformation

$$r^2 = \rho^2 - r_+^2 \quad (25)$$

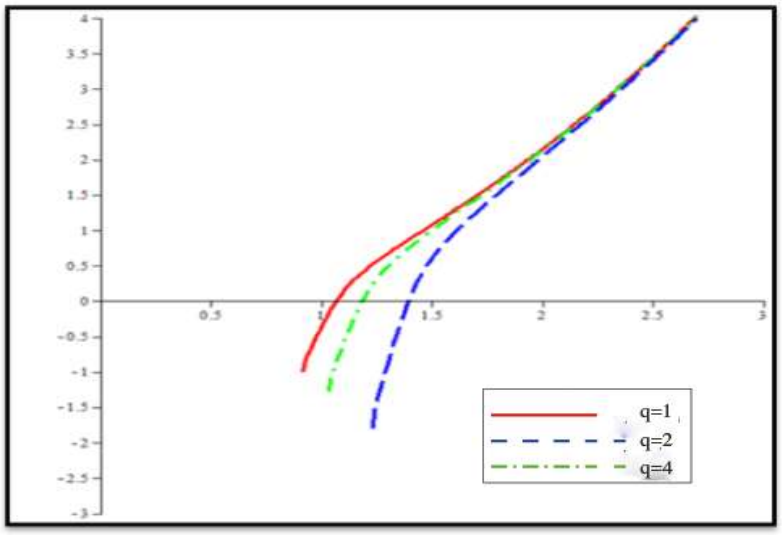

Figure 1. $f(\rho)$ versus ρ with $M = 5$, $\beta = 10$, $n = 4$, $\lambda = -\cdot/\cdot\setminus$, $\mu = 0.4$, and $c = -0.01$.

In Fig. 1, $f(\rho)$ versus ρ for different values of q and for Exponential nonlinear electrodynamic is plotted. As mentioned, there is a r_+ which $f(\rho) < 0$ for $\rho < r_+$ and unacceptable. Also, for constant values of parameters M, β, n, λ, μ and c, when we increase the value of q, the value of r_+ increases. The function f has a constant value for each value of ρ, but in the region near r_+, as q increases it decreases.

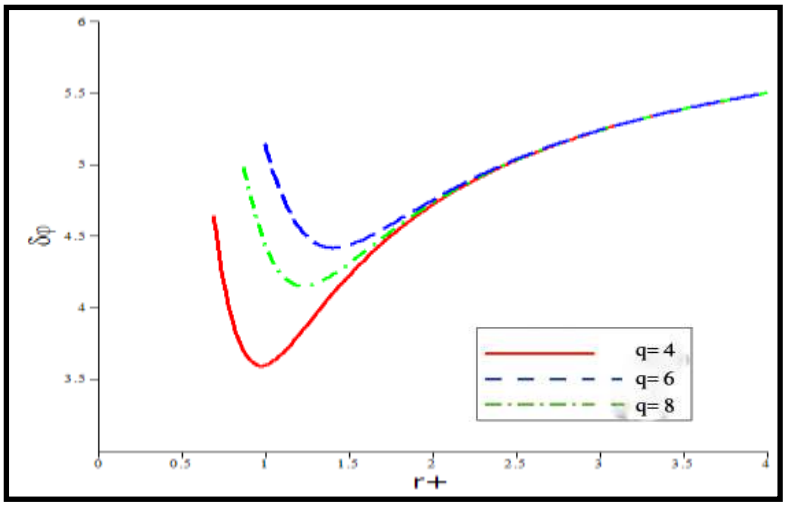

Figure 2. $\delta\phi$ versus r_+ with $\beta = 10$ and $n = 4$.

In Fig. 3, for different values of q, there is a minimum value for r_+ that $\delta\phi$ is real only for $r_+ > r_{+min}$ and the same way for $r_+ > r_{+max}$, $\delta\phi$ is independent of q and has a constant value for each value of r_+. While in the range of $r_{+min} < r_+ < r_{+max}$, $\delta\phi$ depends on the value of q and as q increases it increases.

4 Concluding Results

In this paper, we obtained magnetic solutions of quartic quasi-topological gravity in the presence of nonlinear electrodynamic exponential generated by a rotating magnetic brane. It should be noted that quasi-topological gravity is a higher derivative theory and has no limitations on dimensions. So, if we consider the parameters of quasi-topological gravity zero ($\lambda = \mu = c = 0$) this theory reduces to Einstein's theory and also reduces to linear Maxwell field, if the nonlinearity parameter β goes to infinity. These solutions have no curvature singularity and no horizons, but have conical singularity with a deficit angle. The function f is defined in the range $r_+ < \rho < \infty$ and does not contain the point $\rho = 0$. In the continue, we analyze the behaviors of the function f for the various parameters.

References

[1] S. H. Hendi, "Asymptotic charged BTZ blach hole solutions", JHEP 03 (2012).

[2] A. Shykhi, F. Naeimipour and S. M. Zebarjad, "Thermodynamic geometry and thermal stability of n-dimensional dilaton black holes in the presence of logarithmic nonlinear electrodynamics", Phys. Rev. D 92, 124054 (2015).

[3] A. Shykhi, F. Naeimipour and S. M. Zebarjad, "Phase transition and thermodynamic geometry of topological dilaton black holes in gravitating logarithmic nonlinear electrodynamics", Phys. Rev. D 91, 124057 (2015).

[4] A. Bazrafshan, F. Naeimipour, M. Ghanaatian, GH. Forozani and A. Alizadeh, "Dilaton black holes coupled to nonlinear electrodynamic field", Phys. Rev. D 89, 104019 (2014).

[5] A. Shykhi and S. Hajkhalili, "Dilaton black holes coupled to nonlinear electrodynamic field", Phys. Rev. D 89, 104019 (2013).

[6] A. Shykhi, F. Naeimipour and S. M. Zebarjad, "Quasitopological magnetic brane coupled to nonlinear electrodynamics", Phys. Rev. D 99, 124009 (2019).

[7] M. Ghanaatian, A. Bazrafshan and W.G. Berenna, “Lifshitz quartic quasitopological black holes”, Phys. Rev. D 9, 124012 (2014).

[8] M. Ghanaatian, F. Naeimipour, A. Bazrafshan and M. Abkar, “Charged black holes in quartic quasi-topological gravity”, Phys. Rev. D 97, 104054 (2018).

[9] M. Ghanaatian, A. Alizadeh, A. Bazrafshan and GH. Forozani, “Spining Magnetic Brane of Quartic Quasi-Topological Gravity in the Presence of Nonlinear Electrodynamics”, Iranian Journal of Astronomy and Astrophysics 5 (2) 83-98 (2018).

Abstract paper - Poster

Constraining Holographic Dark Energy Models with Current Cosmological Observations

Sonali Borah
Department of Physics, Assam University, Silchar-788011, Assam, India
Email: sonalicosmo@gmail.com

Abstract. The accelerating expansion of the universe remains one of the most profound discoveries in modern cosmology, motivating a wide class of dark energy models to explain it. Among these, the holographic dark energy (HDE) model, which is based on the holographic principle of quantum gravity, offers a fascinating framework for explaining cosmic acceleration in the late time. In this paper, we jointly analyze recent cosmological datasets, such as gamma-ray burst distance indicators, cosmic chronometer (CC) measurements of the Hubble parameter, and Type Ia supernovae from the Pantheon sample, to present observational constraints on HDE models. We constrain the HDE parameters using Markov Chain Monte Carlo methods and a Bayesian statistical framework. Our findings show that late-time cosmic acceleration can still be explained by HDE models. These findings highlight how crucial holographic methods are for examining the nature of cosmic acceleration and dark energy.

References

[1] S. Perlmutter, G. Aldering, G. Goldhaber, et al., “Measurements of Ω and Λ from 42high-redshift supernovae,” Astrophys. J. 517, 565 (1999).

[2] L. Susskind, “The world as a hologram,” J. Math. Phys. 36, 6377 (1995).

[3] E. N. Saridakis, “Barrow holographic dark energy,” Phys. Rev. D 102, 123525 (2020).

[4] D. Scolnic, B. Popovic, A. Riess, et al., “The Pantheon+ analysis: Cosmological con-straints,” Astrophys. J. 938, 113 (2022).

[5] M. Demianski, E. Piedipalumbo, C. Rubano, P. Scudellaro, “Cosmology with gamma-ray bursts. II. Cosmography challenges and cosmological scenarios,” Astron. Astrophys.598, A113 (2017).

[6] A. G. Riess et al., “A Comprehensive Measurement of the Local Value of the HubbleConstant with 1 km s−1 Mpc−1 Uncertainty from the Hubble Space Telescope and theSH0ES Team,” Astrophys. J. Lett. 934, L7 (2022).

[7] H. Wei, R. G. Cai, “A new model of agegraphic dark energy,” Phys. Lett. B 660, 113(2008).

[8] C. Gao, F. Wu, X. Chen, Y. G. Shen, “A holographic dark energy model from Ricciscalar curvature,” Phys. Rev. D 79, 043511 (2009).

Proceedings of the 4th International Conference on Holography and its Applications

18 to 19 September, 2025, Khazar University, Baku, Azerbaijan. ICHA4(2025)303

Full paper – Poster

A Higher-Dimensional Approach to the Hubble Constant Anomaly

E. Naghde Mezerji[1], F. Ahmadi[2]
[1]Department of Physics, Shahid Rajaee Teacher Training University, Lavizan, Tehran 16788, Iran
Email: e.n.mezerji@sru.ac.ir
[2]Department of Physics, Shahid Rajaee Teacher Training University, Lavizan, Tehran 16788, Iran
Email: fahmadi@sru.ac.ir

Abstract. In this paper, we studied the Hubble parameter via the Brane models. In these models, the interaction of the Brane and Bulk causes an energy exchange between them. Here, we used the power-law potential as the initial dark energy. Our results show that the energy exchange and potential energies have the significant impact on the accelerated expansion of the universe in late time and Hubble tension. We then examined the cosmological parameters that represent slow-roll inflation.

1 Introduction

Modern cosmology is based on a fundamental principle: our universe is not only expanding, but this expansion is accelerating over time. This expansion is described by a quantity called the Hubble constant (H_0). The Hubble parameter tells us how fast the universe is expanding. For decades, scientists have had two main ways to calculate this constant: A. The direct method (local cosmology): This method relies on observing “nearby” objects such as Cepheid variables and type Ia supernovae in neighboring galaxies. By measuring their speed of receding (via the galactic redshift), the Hubble parameter is calculated directly. B. The indirect method (early cosmology): This method looks back in time, to just 380,000 years after the Big Bang, rather than looking at the present-day universe. By carefully examining the cosmic microwave background (CMB), which is a fossilized map of the infant universe and recorded by satellites such as Planck, cosmological parameters can be extracted. Using the Standard Model of Cosmology (ΛCDM), which includes dark energy and cold dark matter, it is possible to predict what these parameters would ultimately lead to in the present-day universe. For years, it was expected that these two independent methods would arrive at a single value for the Hubble parameter. But this did not happen. This is precisely the starting point of the "Hubble tension." Various methods have been proposed to resolve this tension [1-3].

To explain this tension theoretically, we use Brane cosmological models. For the unification of general relativity (which describes the macroscopic universe) and quantum mechanics (which describes the world of subatomic particles), bold and revolutionary new theories have emerged. One of the most exciting and imaginative of these theories is brane cosmology. This theoretical framework has its roots in string theory, specifically M-theory, and proposes a fundamental and surprising idea. The three-dimensional universe we inhabit is actually a multidimensional brane floating in a higher-dimensional, more expansive spacetime called the bulk. All particles and forces of the Standard Model (except gravity) are confined to the surface of this brane and cannot leak into higher dimensions. But gravity, unlike other forces, is not confined to the brane and can spread throughout the multidimensional bulk. By providing this new framework, brane cosmology offers innovative solutions to some of the deepest mysteries of cosmology, including the nature of dark energy and dark matter. In fact, these mysterious

phenomena could be related to the interaction of our universe with extra dimensions and cosmic inflation. The period of rapid exponential expansion of the universe in the first moments after the Big Bang was caused by the collision of our brane with another brane. As a result, brane cosmology is not just an abstract theory, but a bridge between particle physics and cosmology [4-7].
In this paper, we first introduce our action. Then we derive the Friedmann equations. The results indicate that energy is transferred between the bulk and the brane. Next, we calculate the cosmological parameters. These parameters fit well with the CMB data and indicate slow-roll inflation. Additionally, the examination of the Hubble parameter reveals an increase in late times, which supports its agreement with the Hubble tension and observational data.

2 The Bulk-Brane Interaction

The model we are considering features a 5-dimensional space-time bulk, where scalar fields ϕ are located, and a 4-dimensional brane, where material fields ψ are situated. These two fields are coupled by $\tilde{h}_{\alpha\beta} = A^2(\phi)h_{\alpha\beta}$ [4-7],

$$S = \frac{1}{2}\int d^5s\sqrt{-g}(R - g^{ab}\nabla_a\phi\nabla_b\phi - 2V(\phi)) + \int d^4sL_m\,(\psi_m, A^2(\phi)h_{\alpha\beta}) \quad (1)$$

Where g_{ab} is the space-time metric 5D and $h_{\alpha\beta}$ is the space-time metric 4D,

$$dS^2 = g_{ab}dx^a\mathrm{d}x^b = h_{\alpha\beta}dx^\alpha\mathrm{d}x^\beta + \gamma^2(t,y)dy^2 \quad (2)$$

Here, we use the 5D FRW metric to study the cosmology of our model.

$$dS^2 = -n^2(t,y)dt^2 + a^2(t,y)\left[\frac{dr^2}{1-kr^2} + r^2(d\theta^2 + \sin^2\theta\, d\varphi^2)\right] + \gamma^2(t,y)dy^2 \quad (3)$$

Where $k = 0, \pm 1$. By the calculus of variations, we can obtain the Einstein equations and by using the metric, the Friedmann equations of the model. Then, by combining the Friedmann equations, we have

$$\dot{H} + H^2 = \frac{1}{12}\left[\frac{\zeta(1-3\omega_\gamma)\rho_\gamma}{H} - (\rho_\phi + 3P_\phi)\right] - \frac{1}{36}{\rho_\gamma}^2\left[\frac{\zeta(1-3\omega_\gamma)}{H} + 3\omega_\gamma + 2\right]. \quad (4)$$

Where $H = \frac{\dot{a}}{a}$, $\rho_\phi = \frac{1}{2}\dot{\phi}^2 + V(\phi)$, $P_\phi = \frac{1}{2}\dot{\phi}^2 - V(\phi)$, $\zeta = \frac{d\ln A(\phi)}{d\phi}$, $\rho_\gamma = -\frac{6}{a\gamma}(\frac{\partial a}{\partial y})$, $\omega_\gamma = \frac{P_\gamma}{\rho_\gamma}$. The above equation indicates that the standard model of cosmology is altered by the influence of the bulk scalar on the dynamics of the brane. The coupling of matter and scalar fields by the metric of the brane leads to an energy exchange between the bulk and the brane. This exchange of energy can play an important role in Hubble tension. On the other hand, the equation of scalar field ϕ on the brane is calculated as follows: if we consider $\omega_\gamma = -1$ and $\dot{\gamma} = 0$, we can obtain,

$$\ddot{\phi} + 3H\dot{\phi} + \frac{dV(\phi)}{d\phi} = 4\zeta\rho_\gamma \quad . \quad (5)$$

Also, the energy density of scalar field in the bulk and the energy density of matter field on the brane are calculated as follows,

$$\dot{\rho_\phi} + 3H\rho_\phi + 3H\omega_\phi\rho_\phi = 4\zeta\dot{\phi}\rho_\gamma\,, \quad (6)$$

$$\dot{\rho_\gamma} = -4\zeta\dot{\phi}\rho_\gamma \quad . \tag{7}$$

The other assumption is that brane energy density is the result of matter and vacuum energy $\rho_\gamma = \rho_m + \rho_\Lambda$, we have [5],

$$\rho_\Lambda = \rho_{\Lambda_0} e^{-4\zeta\phi} \quad . \tag{8}$$

Also, the effective potential on the brane is $V_{eff} = V + \rho_\Lambda$.

3 Inflation on the Brane

In this section, we specifically study the Power-Low potential [1-3]. According to the results obtained in the previous section, we have,

$$V_{eff} = V_0 \frac{\phi^{2n}}{2^n} + \rho_{\Lambda_0} e^{-4\zeta\phi} \quad . \tag{9}$$

Here, we assume the coupling of the interaction between the bulk and the brane to be a function of the scalar field as

$$\zeta = \phi \, . \tag{10}$$

First, we plot the effective potential based on the scalar bulk field for ($n = 1,2,3$).

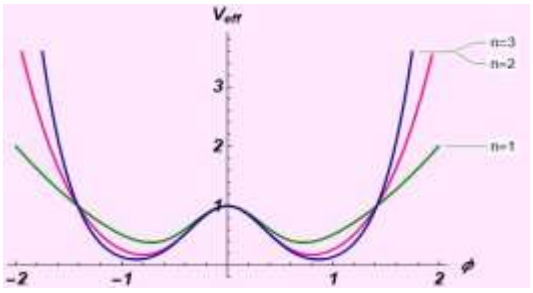

Figure 1. Plot (V_{eff}, ϕ) for $n = 1,2,3$.

Fig. 1 shows the variations of dark energy in terms of the bulk scalar field. In this representation, the minima of dark energy can rest in two potential wells. At $\phi \leq -1$, the energy is initially active and goes from fast-roll to slow-roll. It then reheats and at $-1 < \phi < 1$ it slowly rolls to $\phi = 1$ and reheats again. The bulk scalar field energy can also oscillate around 1 and -1 and decompose into Standard Model particles. In this paper, we consider slow rolling inflation to investigate the effect bulk-brane interactions on the Hubble tension. In this case, the rolling speed is $\dot{\phi} = \frac{-V_{eff}{}'}{3H}$. To examine it more precisely, we plot the rolling speed based on the block scalar field.

$$\dot{\phi} = \frac{-n2^{1-n}\phi^{2n-1}V_0 + 8e^{-4\phi^2}\phi\rho_{\Lambda_0}}{3\sqrt{\frac{V_0}{6}2^{-n}\phi^{2n} - \frac{{\rho_{\Lambda_0}}^2}{36}e^{-8\phi^2}}} \tag{11}$$

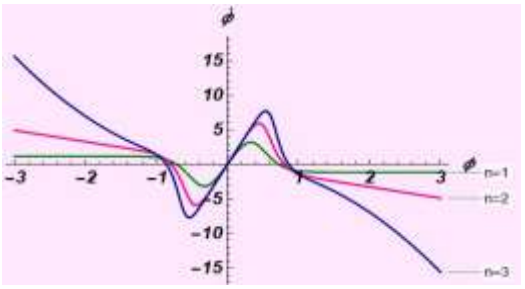

Figure 2. Plot $(\dot{\phi}, \phi)$ for $n = 1,2,3$.

According to Fig. 2 in negative scalar fields, the velocity is decreasing. We have an accelerating contraction at $-\infty < \phi < 0.4$. Then the expansion velocity increases, and we have an accelerating expansion at $-0.4 < \phi < 0.4$. Finally, it decreases again at $0.4 < \phi < \infty$. Now, we examine the cosmological parameters. First, we calculate the first and second parameters of slow rolling. Then we plot them in Fig. 3. In conditions $\varepsilon < 1$ and $|\eta| < 1$, we have inflation.

$$\varepsilon = \frac{1}{2}\left(\frac{n2^{1-n}\phi^{2n-1}V_0 - 8e^{-4\phi^2}\phi\rho_{\Lambda_0}}{2^{-n}\phi^{2n}V_0 - e^{-4\phi^2}\rho_{\Lambda_0}}\right)^2 \tag{12}$$

$$\eta = \frac{(2n-1)n2^{1-n}\phi^{2n-2}V_0 - 8e^{-4\phi^2}(8\phi^2-1)\rho_{\Lambda_0}}{2^{-n}\phi^{2n}V_0 - e^{-4\phi^2}\rho_{\Lambda_0}} \tag{13}$$

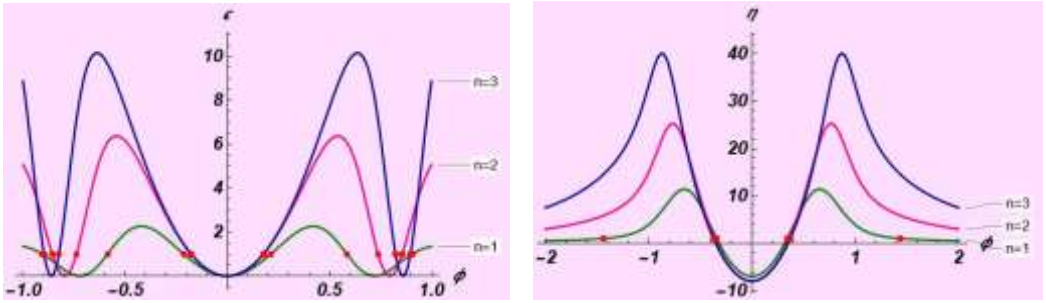

Figure 3. Plot (ε, ϕ) and (η, ϕ) for $n = 1,2,3$.

In the following, we calculate two parameters, the spectral index (n_s) and the tensor-to-scalar ratio (r). According to the CMB data, these two parameters should be about $n_s \approx 0.965$ and $r < 0.036$.

$$\mathrm{r} = 8\left(\frac{n2^{1-n}\phi^{2n-1}V_0 - 8e^{-4\phi^2}\phi\rho_{\Lambda_0}}{2^{-n}\phi^{2n}V_0 - e^{-4\phi^2}\rho_{\Lambda_0}}\right)^2 \tag{14}$$

$$n_s = 1 + \frac{(2n-1)n2^{2-n}\phi^{2n-2}V_0 - 16e^{-4\phi^2}(8\phi^2-1)\rho_{\Lambda_0}}{2^{-n}\phi^{2n}V_0 - e^{-4\phi^2}\rho_{\Lambda_0}} - 3\left(\frac{n2^{1-n}\phi^{2n-1}V_0 - 8e^{-4\phi^2}\phi\rho_{\Lambda_0}}{2^{-n}\phi^{2n}V_0 - e^{-4\phi^2}\rho_{\Lambda_0}}\right)^2 \tag{15}$$

Finally, we have calculated the values of these parameters for different cases (n = 1, 2, 3) and placed them in Table 1.

Table 1. The values of inflationary parameters.

	$\varepsilon < 1$	$\lvert\eta\rvert < 1$	ε	η	r	$n_s \approx 1$
n=1	*-0.215* $< \phi <$ 0.213	*0.293* $< \phi <$ 0.342	8.8×10^{-6}	-0.0274	0.0014	0.945
n=2	*-0.177* $< \phi <$ 0.177	*0.319* $< \phi <$ 0,361	4.1×10^{-6}	-0.0338	6.6×10^{-5}	0.932
n=3	*-0.177* $< \phi <$ 0.177	*0.328* $< \phi <$ 0.372	7.2×10^{-7}	-0.0427	1.1×10^{-5}	0.914

4 Anomaly Analysis

In this section, we will examine the Hubble parameter. The Hubble expansion rate is proportional to the potential energy $H^2 \propto V(\varphi)$. Using equation (8), (9) and (10), the first Friedman equation of the model becomes

$$H^2 = \frac{V_0}{6}\frac{\phi^{2n}}{2^n} + \frac{\rho_{\Lambda_0}}{36}e^{-8\phi^2} \tag{16}$$

Now, we plot H, Fig. 4. According to this figure, the Hubble parameter increases as the bulk scalar field increases.

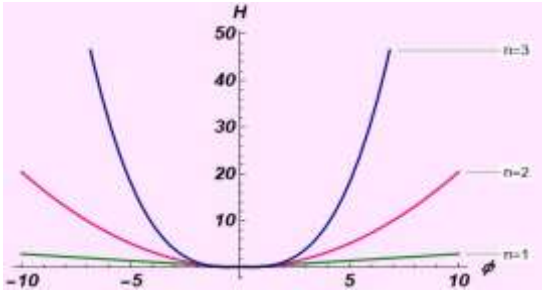

Figure 4. Plot (H, ϕ) for $n = 1,2,3$.

If we assume the bulk scalar field ϕ as

$$\phi = -\frac{\alpha}{\ln a} \qquad a = \frac{1}{1+z} \tag{17}$$

where z is the redshift, we can plot the Hubble parameter as a function of redshift in Fig. 5. The plot shows an increase in the Hubble parameter at the last time (z=1), which is in perfect agreement with the observational data.

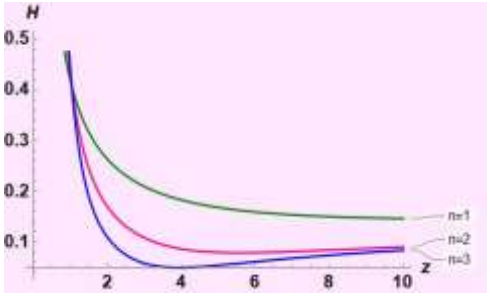

Last Time

Figure 5. Plot (H, z) for $n = 1,2,3$ and $\alpha = 1$.

Now, we examine equation (9) again and plot the effective potential based on the variables of equation (17), where we just replaced a with $\frac{a}{a_i}$ and a_i is initial scale factor (after the Big Bang). This graph shows the decreasing trend of the potential (U_{eff}) with increasing scale factor. In this case, our solution provides a beautiful explanation of the Hubble tension (Fig. 6).

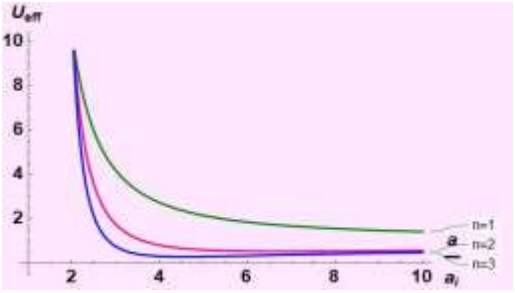

Figure 6. Plot (U_{eff}, z) for $n = 1,2,3$, $V_0 = 10$ and $\alpha = 1$.

5 Conclusions

We considered a brane universe where a 3+1D brane is contained within a 4+1D bulk. Then we write Friedmann's equations, and the results showed energy transfer between the bulk and the brane [5]. We also used a power-law potential for primordial dark energy. This potential could solve the Hubble tension [1-3]. The interaction energy, along with dark energy, well demonstrates the accelerating expansion of the universe. We also calculated the cosmological parameters and put them in Table 1. Our results predict slow-roll inflation and agree with the CMB data. Finally, by studying the Hubble parameter, considering $\phi = -\alpha\,(\ln a)^{-1}$, we can observe its increase in last time, indicating its agreement with observational data.

References

[1] Eleonora Di Valentino *et al* 2021 *Class. Quantum Grav.* 38 153001

[2] Chudaykin A, Gorbunov D and Nedelko N 2020 JCAP 08 013 [arXiv:2004.13046]

[3] Joudaki S et al. 2020 Astron. Astrophys. 638 L1 [arXiv:1906.09262]

[4] Y. Bisabr, “Hubble tension in power-law f(R) gravity and generalized Brans-Dicke theory,” Int. J. Mod. Phys. D (2025), [arXiv:2403.13303]

[5] Y. Bisabr, F. Ahmadi, “Deflation of Vacuum Energy During Inflation Due to Bulk-Brane Interaction,” JCAP 10 (2020) 050.

[6] Y. Bisabr and F. Ahmadi, Phys. Lett .B 774, 671 (2017)

[7] Y. Bisabr, “Chameleon Brans-Dicke cosmology,” Phys. Rev. D 86 (2012) 127503.

Proceedings of the 4th International Conference on Holography and its Applications

18 to 19 September, 2025, Khazar University, Baku, Azerbaijan. ICHA4(2025)304

Full paper – Poster

Exponential Corrected Thermodynamics of Massive Black Holes on the Brane

Hoda Farahani[1]
[1]School of Physics, Damghan University, Damghan, 3671641167, Iran
Email: h.farahani@du.ac.ir

Abstract. We investigate the thermodynamic properties of massive black holes on a two-dimensional brane embedded in a three-dimensional bulk spacetime, focusing on exponential corrections to the black hole entropy. Using the doubly holographic braneworld framework, we analyze the black hole metric derived from BTZ geometry with backreacting branes. The system exhibits rich thermodynamic behavior where the black hole entropy receives non-perturbative exponential corrections of the form $S_c = S + \alpha e^{-S}$. We compute the temperature, entropy, and energy of the braneworld black holes and examine their modified thermodynamic properties. Our results demonstrate how quantum corrections fundamentally alter the thermodynamic stability and phase structure of these gravitational systems, providing new insights into the interplay between quantum effects and gravity in lower-dimensional models.

1 Introduction

The study of black hole thermodynamics has been a cornerstone of theoretical physics, providing crucial insights into the fundamental nature of gravity, quantum mechanics, and information theory. In recent years, doubly holographic models have emerged as powerful tools for understanding black hole physics, particularly in the context of the information paradox and the Page curve [1-3]. The AdS/CFT correspondence has revolutionized our understanding of quantum gravity by establishing a duality between gravitational theories in the bulk and conformal field theories on the boundary [4]. This holographic principle has been extended to include braneworld scenarios, where lower-dimensional gravitational systems emerge as effective theories on codimension-one surfaces embedded in higher-dimensional spacetimes. Of particular interest are massive black holes in braneworld models, which exhibit novel thermodynamic properties not present in their higher-dimensional counterparts. These systems provide a controlled setting for investigating quantum corrections to black hole thermodynamics, including exponential corrections that arise from quantum fluctuations and non-perturbative effects. The motivation for studying exponential corrections stems from various approaches to quantum gravity, including string theory and loop quantum gravity, which predict modifications to the Bekenstein-Hawking entropy formula. These corrections are particularly important near extremal limits and in regimes where quantum effects become significant. In this work, we investigate a specific class of exponential corrections to black hole entropy in the context of braneworld models. We focus on massive black holes that arise from BTZ geometries with backreacting branes, providing a concrete realization of quantum-corrected black hole thermodynamics.

2 Black Hole Metric and Braneworld Setup

We begin with the BTZ black hole metric in three-dimensional Anti-de Sitter space [5,6],

$$ds^2 = -\left(\frac{r^2}{L^2} - \mu^2\right)\frac{L^2}{r^2}dt^2 + \left(\frac{1}{\frac{r^2}{L^2}-\mu^2} + \frac{k^2}{\frac{r^2}{L^2}+k^2\mu^2}\right)dr^2 \quad (1)$$

where L is the AdS radius, μ is a parameter related to the black hole mass, r is the boundary cylinder radius, and k characterizes the brane tension through the relation,

$$k = \sqrt{\frac{4\pi G_N L T_0}{1-16\pi^2 {G_N}^2 L^2 {T_0}^2}} \quad (2)$$

Here G_N is Newton's constant and T_0 is the brane tension. The brane extends across the Einstein-Rosen bridge, intersecting the asymptotic boundaries at $\phi = 0$. The brane profile is determined by the Israel junction conditions and takes the form:

$$\sinh \mu\phi = \frac{k\mu L}{r} \quad (3)$$

This profile ensures that the brane reaches the boundary at the specified locations while satisfying the appropriate junction conditions across the brane surface.

3 Thermodynamics of the Braneworld Black Hole

The fundamental thermodynamic quantities of the braneworld black hole can be computed using standard methods. The temperature is given by:

$$T = \frac{\mu}{2\pi R}, \quad (4)$$

This temperature characterizes the thermal state of the boundary CFTs and determines the thermal properties of the entire system. The uncorrected entropy follows from the area law:

$$S = \frac{2\pi^2}{3}cRT + \frac{c}{3}\ln 2k \quad (5)$$

where $c = 3L/(2G_N)$ is the central charge of the boundary CFT. The first term represents the thermal entropy of the boundary theory, while the second term is the defect contribution arising from the presence of the brane. The energy of the system is,

$$S = \frac{\pi^2}{3}cRT^2 \quad (6)$$

4 Non-perturbative correction

The key result of our analysis concerns exponential corrections to the black hole entropy. These corrections arise from quantum fluctuations and non-perturbative effects that become important in certain regimes of the parameter space. The corrected entropy takes the form:

$$S_c = S + \alpha e^{-S} \quad (7)$$

where α is a parameter that depends on the specific quantum theory under consideration and the microscopic details of the black hole. This exponential correction represents a fundamental departure

from the classical Bekenstein-Hawking formula and has important implications for black hole thermodynamics, particularly in understanding the approach to extremality and the behavior of the entropy in quantum regimes.

The exponential correction in equation (7) can be understood from several perspectives that converge to highlight the underlying quantum structure of spacetime. One interpretation attributes the correction to quantum fluctuations of the gravitational field near the black hole horizon, which become significant when the classical entropy is not overwhelmingly large. From an information-theoretic standpoint, the correction captures the discreteness of the underlying quantum degrees of freedom and the finite dimensionality of the Hilbert space. Furthermore, within the framework of holography, this correction reflects the finite nature of the boundary theory and the discrete spectrum of the associated conformal field theory. Together, these perspectives underscore the fundamentally quantum and granular character of black hole entropy. The presence of exponential corrections modifies the thermodynamic stability of the black hole. The corrected specific heat becomes:

$$C = T\frac{\partial S_c}{\partial T} = T\frac{\partial S}{\partial T}\left(1 - \alpha e^{-S}\frac{\partial S}{\partial T}\right) \tag{8}$$

This modification can lead to new phases and phase transitions that are absent in the uncorrected theory.

5 Page Curve and Information Theory

In the doubly holographic setup, the system exhibits the characteristic Page curve behavior. The entanglement entropy between the bath and the black hole initially grows linearly with time:

$$S_{early}(t) = \frac{2c}{3}\ln\left(\frac{1}{2\pi\delta T}\right) + \frac{4\pi c}{3}Tt \tag{9}$$

where δ is a UV cutoff in the boundary theory.

At late times, the entanglement entropy saturates due to the formation of quantum extremal islands. The saturation value depends on the relative sizes of the black hole and bath:

$$S_{late} = min(S_{thermal}, S_{island}) \tag{10}$$

where $S_{thermal}$ represents the thermal entropy of the bath and S_{island} includes contributions from the quantum extremal island. There exists a critical bath size that determines the transition between different late-time behaviors:

$$R_c \propto \frac{\ln 2k}{2\pi T(\pi - 2\phi_\Sigma)} \tag{11}$$

For bath sizes smaller than R_c, the late-time entropy is determined by the thermal bath capacity. For larger baths, quantum extremal islands form and determine the saturation value.

6 Quantum Corrections and Phase Structure

The exponential corrections significantly modify the phase structure of the black hole system. The critical temperature for the Hawking-Page transition becomes:

$$T_c = \frac{1}{\pi^2 R}\left[\sqrt{\frac{\pi^2}{4} + \operatorname{arcsinh}^2 k} - \operatorname{arcsinh} k\right] \tag{12}$$

For large brane tensions (large k), this critical temperature decreases as:

$$T_c \propto \frac{1}{8R \ln 2k} \tag{13}$$

The corrected free energy includes contributions from the exponential correction:

$$F_c = F - T\alpha e^{-S}\frac{\partial S}{\partial T} \tag{14}$$

This modification affects all thermodynamic potentials and can lead to new critical points and phase transitions.

7 Conclusions

Our results highlight that, exponential corrections fundamentally modify the thermodynamic behavior of black holes in braneworld models, revealing deeper aspects of their quantum nature. These corrections not only refine our understanding of black hole thermodynamics but also shed light on the microscopic structure underlying these gravitational systems. Importantly, they play a significant role in addressing the black hole information paradox through the island prescription, as the modified entropy influences key transition times and the critical conditions under which quantum extremal islands emerge. From a holographic standpoint, the findings offer valuable new tools for probing the thermodynamics of strongly coupled quantum systems, capturing non-perturbative effects that are typically inaccessible by other methods. Moreover, the form and implications of these exponential corrections align with predictions from multiple quantum gravity approaches, such as string theory and loop quantum gravity, suggesting a universal character to these modifications. This convergence reinforces the relevance of exponential corrections as a robust feature across diverse formulations of quantum gravity. We have investigated the thermodynamic properties of massive black holes on branes, focusing in particular on the role of exponential corrections to the entropy. Our analysis revealed that these corrections, expressed in the form $S_c = S + \alpha e^{-S}$, arise from fundamental quantum effects and carry important physical implications. They significantly modify the black hole's thermodynamic behavior, altering its stability and phase structure, and introducing new critical points and phase transitions that do not appear in the classical description. Moreover, the exponential corrections influence the dynamics of entanglement, affecting the evolution of the Page curve and contributing to the formation of quantum extremal islands, thereby offering fresh insights into the information-theoretic aspects of black holes. We also identified specific critical parameters—such as bath sizes and temperatures—that delineate different thermodynamic phases, and demonstrated how quantum corrections shift these critical values. From a holographic perspective, our results shed new light on the emergence of spacetime from quantum entanglement and the nature of gravity in a holographic framework. These findings enhance our understanding of quantum black hole thermodynamics and offer valuable tools for probing the deep connections between gravity and quantum mechanics. Looking ahead, future research should extend this analysis to higher-dimensional settings and alternative brane configurations, as well as explore connections with other approaches to quantum gravity. It is important to note that the exponential corrections examined here represent just one category of quantum modifications; a comprehensive understanding of quantum black holes will require a broader analysis of various correction types and how they interact across different physical regimes.

References

[1] G. Grimaldi, J. Hernandez, R. C. Myers, "Quantum Extremal Islands Made Easy, Part IV: Massive Black Holes on the Brane", JHEP 03, 136 (2022)

[2] H. Z. Chen, R. C. Myers, D. Neuenfeld, I. A. Reyes and J. Sandor, "Quantum Extremal Islands Made Easy, Part I: Entanglement on the Brane", JHEP 10, 166 (2020)

[3] H. Z. Chen, R. C. Myers, D. Neuenfeld, I. A. Reyes and J. Sandor, "Quantum Extremal Islands Made Easy, Part II: Black Holes on the Brane", JHEP 12, 025 (2020)

[4] J. M. Maldacena, "The Large N limit of superconformal field theories and supergravity", Adv. Theor. Math. Phys. 2, 231 (1998)

[5] M. Banados, C. Teitelboim and J. Zanelli, "The Black hole in three-dimensional space-time", Phys. Rev. Lett. 69, 1849 (1992)

[6] S. Carlip, "The (2+1)-Dimensional black hole", Class. Quant. Grav. 12, 2853 (1995)

[7] A. Almheiri, N. Engelhardt, D. Marolf and H. Maxfield, "The entropy of bulk quantum fields and the entanglement wedge of an evaporating black hole", JHEP 12, 063 (2019)

[8] D. N. Page, "Information in black hole radiation", Phys. Rev. Lett. 71, 3743 (1993)

[9] S. Ryu and T. Takayanagi, "Holographic derivation of entanglement entropy from AdS/CFT", Phys. Rev. Lett. 96, 181602 (2006)

[10] T. Hartman and J. Maldacena, "Time Evolution of Entanglement Entropy from Black Hole Interiors", JHEP 05, 014 (2013)

Abstract paper – Poster

Simulating Bubbles in a Holographic QCD-like Phase Diagram

Yago Bea[1], Mauro Giliberti [2] , David Mateos[3], Mikel Sanchez-Garitaonandia[4]
Alexandre Serantes[5], Miguel Zilhão[6]
[1] Departament de F´ısica Qu`antica i Astrof˜ısica and Institut de Ci`encies del Cosmos (ICC),
Universitat de Barcelona, Mart´ı i Franqu`es 1, ES-08028, Barcelona, Spain.
Email: yagobea@icc.ub.edu
[2] Dipartimento di Fisica e Astronomia, Universit`a degli Studi di Firenze; Via G. Sansone 1; I-50019
Sesto Fiorentino (Firenze), Italy.
Email: mauro.giliberti@unifi.it
[3] Institució´ Catalana de Recerca i Estudis Avan¸cats (ICREA), Passeig Llu´ıs Companys 23,
ES-08010, Barcelona, Spain.
Email: dmateos@fqa.ub.edu
[4] CPHT, CNRS, ´Ecole polytechnique, Institut Polytechnique de Paris, 91120 Palaiseau, France.
Email: mikel.sanchez@polytechnique.edu
[5] Department of Physics and Astronomy, Ghent University, 9000 Ghent, Belgium.
Email: alexandre.serantesrubianes@ugent.be
[6] Centre for Research and Development in Mathematics and Applications (CIDMA),
Department of Mathematics, University of Aveiro, 3810-193 Aveiro, Portugal.
Email: mzilhao@ua.pt

Abstract. A line of first-order phase transitions is conjectured in the phase diagram of Quantum Chromodynamics at non-zero baryon density. If this is the case, numerical simulations of neutron star mergers suggest that various regions of the stars may cross this line multiple times. This results in the nucleation of bubbles of the preferred phase, which subsequently expand and collide. The resulting gravitational wave spectrum is highly sensitively to the velocity of the bubble walls. We use holography to perform the first microscopic simulation of bubble dynamics in a theory that qualitatively mirrors the expected phase diagram of Quantum Chromodynamics. We determine the wall velocity in the metastable regions and we compare it to theoretical estimates. We discuss implications for gravitational wave production.

References

[1] Y. Bea, M. G., D. Mateos, M. Sanchez-Garitaonandia, A. Serantes, and M. Zilhão, "Bubble dynamics in a QCD-like phase diagram", [2412.09588]
[2] M. Sanchez-Garitaonandia and J. van de Vis, "Prediction of the bubble wall velocity for a large jump in degrees of freedom", [2312.09964]
[3] Y. Bea, J. Casalderrey-Solana, T. Giannakopoulos, A. Jansen, D. Mateos, M. Sanchez-Garitaonandia and M. Zilhão ,"Holographic bubbles with Jecco: expanding, collapsing and critical" JHEP09 (2022) 008
[4] O. DeWolfe, S. S. Gubser and C. Rosen, "A holographic critical point", Phys. Rev. D 83, 086005

Abstract paper – Poster

Holographic Complexity for Accelerating AdS Black holes

M. Tavakoli[1], B. Mirza[1], N. Vakili Sarvaghaji[1]
[1]Department of Physics, Isfahan University of Technology, Isfahan 84156-83111, Iran.
Email: Tavakoli.phy@gmail.com
Email: b.mirza@iut.ac.ir
Email: n.vakili@alumni.iut.ac.ir

Abstract. In the framework of AdS/CFT duality, entropy and complexity play pivotal roles in understanding the deep connections between gravity and quantum information theory. This paper explores holographic complexity through the lens of complexity-action duality, focusing on four-dimensional accelerated AdS black holes. We analyze the behavior of complexity in these spacetimes and discuss the implications of our findings for the broader understanding of holographic principles and quantum gravity. Our findings reveal an inverse relationship between the growth rate of complexity and the degrees of freedom of accelerated black holes.

References

[1] S. W. Hawking,"Particle creation by black holes", Comm. Math. Phys. 43(3): 199-220 (1975)

[2] Jacob D. Bekenstein, "Black Holes and Entropy", Phys. Rev. D 7, 2333 (1973).

[3] J. Maldacena, "The large N limit of superconformal field theories and supergravity," AIP Conference Proceedings, vol.484, no.1, pp.51–63, (1999).

[4] M. Natsuume. AdS/CFT duality user guide, vol.903. Springer, (2015).

[5] N. Margolus and L. B. Levitin, "The maximum speed of dynamical evolution," Physica D Nonlinear Phenomena, vol.120, pp.188–195,)1998(.

[6] Leonard Susskind, "The Typical-State Paradox: Diagnosing Horizons with Complexity", Fortschritte der Physik, Volume 64, Issue 1 pp. 84-91 (1908).

Proceedings of the 4th International Conference on Holography and its Applications

18 to 19 September, 2025, Khazar University, Baku, Azerbaijan. ICHA4(2025)307

Full paper – Poster

Innovation in the Embrace of Retro Marketing, the Effectiveness of Holograms in Recalling Shopping Memories

Mehrdad Maleki Verki[1], Muhammad Piri[2]

[1] Master's degree graduate, Department of Business Administration, Faculty of Literature and Humanities, Malayer University, Malayer, Iran.
Email: Mehrdad.maleki.verki@gmail.com

[2] Assistant Professor, Department of Business Administration, Faculty of Literature and Humanities,

Malayer University, Malayer, Iran.

Email: m.piri@malayeru.ac.ir

Abstract. Holographic communication is a transformative technology that is reshaping the digital interaction landscape by enabling the creation of realistic, immersive, and interactive 3D experiences. Access to the past is a concern for consumers when dealing with products, and marketers are also aware of this. Effective use of retro marketing in terms of communication (brand, music, and advertising) helps to evoke emotions to revive the past. Many different products on the market, such as music, movies, or television programs, can increase nostalgic feelings in people. Retro itself is a nostalgic memory of the past. An imitation of a style, fashion, or design from the recent past. There is very little research in the joint field of the impact of holographic art on reviving past memories and its impact on product sales. The authors of the article try to explore the possibility of creating new joint working groups or even applied courses or fields of study by opening a new research path in the interdisciplinary field (holographic and retro marketing).

1 Introduction

When the soulful melodies of Umm Kulthum came to life again in Dubai on October 12th and 13th, 2024. Thousands of fans of the Egyptian singer, known as the "Star of the East", saw her memory and the glorious era of Egypt and the Arab world before their own eyes. In this holographic show, the legendary artist, who died in 1957, returned to the stage "Alive". A vivid and captivating presence. With every note, her voice resonates in the hall, accompanied by a live orchestra, and the digital and real worlds blend seamlessly. The audience relived the emotion, passion and depth of her performances, as if time had turned back. For this enchanting experience, a tribute to Umm Kulthum's art, where the past and the present harmoniously blend.

Holography can explain how our brains can pack so many memories into such a small space. Sometimes in our lives, looking at a long-forgotten object, or a particular smell, suddenly causes us to recall scenes from our past lives. The idea of a holographic pattern is another example of memory-evoking tendencies

[2] Corresponding Author

[16]. The enduring appeal of retro marketing lies in its ability to bridge generations, evoking a sense of nostalgia while embracing contemporary relevance [7]. By infusing elements of the past into today's strategies, brands not only differentiate themselves but also create compelling stories that resonate deeply with consumers [12]. Retro marketing is not just a strategy; it is an invitation to celebrate the richness of the past while building brand identities that stand the test of time.

Effective use of retro marketing in terms of communication (brand, music, and advertising) helps evoke emotions to bring the past to life [29]. Nostalgia marketing allows brands to tap into these powerful emotions and create a deep emotional connection with their audience [33].While many businesses employ nostalgia in their marketing strategies [13], knowledge about the effect of nostalgia proneness on consumer behavior is inadequate [17].

This type of marketing can provide meaningful experiences for consumers by using images, sounds, and themes that evoke fond memories of the past. For example, using vintage music, advertisements, or products that are reminiscent of a particular era can help marketers create a stronger connection with their audience. For retro marketing to be effective, visualizing customers' good memories of a brand is of great importance, and it is at this point that embracing retro marketing with holographic science can be well imagined. The sense of familiarity and the rekindling of faded memories by tasting a flavor or smelling a scent[3] perfectly prepares the consumer for a pleasant purchase in the "Present" based on the "Past."

2 Why is nostalgia important for marketers?

In fact, various studies were reviewed to answer this question, which will be discussed later. But we also asked artificial intelligence and it gave an interesting answer!!: "This directly affects brand awareness, loyalty, and ultimately sales."

As we will see, our intelligent friend's answer is not complete! and several aspects are overlooked.

Nostalgia, a sentimental longing for the past, has been shown to enhance emotional well-being, social connectedness, and even cognitive function [٢2]. Modern branding activities by a host of businesses establish a decision-making attention in nostalgia as a practical marketing instrument. Such activities, employed in a widespread diversity of product categories, aim to take consumers back to the past [1٠].

In NBC Universal's (2013)[4] "Brand Power Index" study, which measures the 500 most talked about brands as determined by factors like social media buzz and online searches, brands evoking the past shot to the top of the Index. This suggests that brand nostalgia can be a key driver for consumer brand purchase [5,6]. Little attention, however, has been paid to measuring the complex nature of this construct. More academic research is surely warranted to develop and validate a generalizable measure of brand nostalgia to help companies gauge and track the nuanced components of nostalgia associated with their brands.

Nostalgic advertising is a type of advertising that, by engaging people's emotions and attitudes, becomes a powerful tool in purchasing products. [2]. The brands which are positioned by using nostalgia enjoy higher brand equity, more favorable product decisions [11] and heightened purchase intentions and the positive word of mouth. [10]. There is a positive relationship between marketing nostalgia and consumer

[3] Recent research has shown that our sense of smell is based on what are called osmic frequencies. Baksi's work, on the other hand, had clearly shown that our skin is sensitive to frequencies caused by vibrations, and even went so far as to suggest that the sense of taste is also the result of frequency analysis. (From the book "The Holographic World" by Michael Talbot, translated to Persian by Dariush Mehrjoui)

[4]NBCUniversal is one of the world's leading media and entertainment companies.www.nbcuniversal.com

purchases Intention. [1]. Nostalgia marketing first encouraged nostalgia emotion, then nostalgia emotion transformed into nostalgia cognition, and eventually nostalgia behavior is formed. People buy more nostalgia product to fulfill the role of nostalgia marketing [24,29].

3 Reviving Nostalgia Through Holographic Displays

Holographic displays are being used to evoke nostalgia by generating immersive, 3D visualizations of past objects, environments, or even deceased individuals. This technology merges retro aesthetics with cutting-edge innovation, allowing people to experience a sense of the past in a novel and engaging way. [9,23]. Holographic displays may amplify these effects by providing multisensory, immersive recreations of past experiences. A study by [14] demonstrated that 3D holographic projections of personal memories elicited stronger emotional responses compared to 2D images, activating deeper memory retrieval mechanisms. [31] found that holography may facilitate more vivid and emotionally intense nostalgia compared to traditional media. Holographic Advertising represents a significant leap forward in the way brands engage with consumers. [3].

4 Advertising Based on Nostalgia Tendencies Using Holographic Advertising

Nostalgia tendencies mention to the sentimental longing or reflective affection for the past, often considered by positive emotions diverse with a sense of loss or desire. Study suggests that nostalgia serves psychological functions, such as enhancing disposition, promotion social connectedness, and providing a sense of continuity in one's identity [22,20]. Individuals may involve in nostalgic replication more often during times of transition, loneliness, or uncertainty, as its suggestions comfort and repeats self-worth [30]. Although normally adaptive, extreme nostalgia can occasionally lead to impractical nostalgia of the past, possibly hindering present-day coping [4].

Nostalgia acts as an emotional resource, helping individuals navigate life's challenges by drawing on meaningful past experiences [20]. Research has shown that customers' nostalgic tendencies increase consumers' purchase intentions by influencing positive emotions, brand attachment, brand trust, and brand commitment. [^]. By integrating 3D holographic displays into advertising strategies, companies can create immersive experiences that not only capture attention but also leave a lasting impression. [15].

This innovative approach to marketing takes advantage of human psychology; our brains are wired to respond more actively to 3D moving images, [32]. Which explains why holograms can be so effective at attracting people [3]. Unlike traditional two-dimensional advertising, holographic advertising allows products to be displayed in a way that makes them appear tangible, almost as if they could be touched [21]. This creates a unique opportunity for brands to showcase their products in full detail, from every angle, without the limitations of physical space.

5 Ultimately, The Future Of Retro Marketing Will Depend On The Support Of Holographic Artists

The future of retro marketing will depend significantly on the support of holographic artists, as emerging research highlights the psychological and technological synergies between nostalgia-driven consumer behavior and immersive holographic experiences. Studies in consumer psychology demonstrate that nostalgia enhances brand attachment by activating the brain's reward system [22].

While holographic technology capitalizes on spatial presence and interactivity to deepen emotional engagement [29]. Advances in holographic displays, such as light-field projections [25], enable photorealistic recreations of retro aesthetics, blending vintage appeal with novelty—a key driver of consumer interest [13].

However, ethical concerns arise regarding the use of posthumous holograms, as neural research suggests that hyper-realistic avatars may trigger uncanny valley effects [28], necessitating careful artistic mediation. Thus, holographic artists, equipped with interdisciplinary expertise in archival design, 3D rendering, and cognitive ergonomics, will be essential in crafting ethically sound, emotionally resonant retro campaigns that leverage holography's unique affordances [27].

6 Ethical Considerations

While holographic nostalgia offers emotional benefits, ethical concerns arise regarding hyper realistic simulations of deceased individuals [26]. and potential over-reliance on virtual nostalgia over real-world engagement. But as we embrace these advancements, we must do so with caution. We must balance technological progress and our ethical responsibility to those whose likenesses we project. AI holograms can enhance our experiences and allow us to engage with the past in ways we never thought possible, but they also force us to consider how we want to remember and celebrate those who have come before us .Holograms have the power to both honor and exploit. As we navigate this exciting yet uncertain future, we must tread carefully, ensuring that our use of this technology aligns with the respect and dignity we owe to the legacies we seek to preserve .One thing is clear: holograms, like the legends they portray, will continue to capture our imagination and redefine how we experience the past and present. Whether we are enthralled or uneasy, we're standing at the edge of a new frontier where technology can bring memories to life in ways we're only beginning to understand.

References

[1] Alkhafagi, Y. A. M. (2023). The Effect of Nostalgia Marketing on Consumers' Purchase Intention. Journal of Economics and Administrative Sciences, 29(136), Article 136.

[2] Bagheri, Mehdi, and Ghiyasabadi Farahani, Maryam. (2018). Investigating the effect of nostalgic advertising on purchase intention with regard to the mediating role of perceived self-persistence, brand attitude, and emotional response to the brand (case study: clean products). Marketing Management, 13(40), 83-94.

[3] Baltezarević, Radoslav & Baltezarevic, Ivana. (2023). Benefits of using holograms in marketing communication. INTERNATIONAL IZMIR ECONOMICS CONGRESS

[4] Batcho KI. (2013) Nostalgia: retreat or support in difficult times? Am J Psychol. 2013 Fall;126(3):355-67 .

[5] Braun-LaTour, K. A., LaTour, M. S., & Zinkhan, G. M. (2007). Using Childhood Memories to Gain Insight into Brand Meaning. Journal of Marketing, 71(2), 45-60 .

[6] Brown, Stephen & Kozinets, Robert & Sherry, John. (2003). Teaching Old Brands New Tricks: Retro Branding and the Revival of Brand Meaning. Journal of Marketing - J MARKETING. 67. 19-33. 10.1509/jmkg.67.3.19.18657.

[7] Chen, Boyi. (2023). Exploring the Revival of Nostalgia and Retro Waves in Contemporary Marketing and Contagious Communication Research—Taking Contagious Möbius Strip as an Example. Highlights in Business, Economics and Management. 23. 958-970. 10.54097/3zyad735.

[8] Esanloo, Bahareh, Khodami, Soheila, and Boroujerdian, Sepideh. (2019). Investigating the effect of fantasy and alienation tendencies on consumers' purchase intention with an emphasis on nostalgia tendencies and brand heritage. Modern Marketing Research, 8(4), 95-110.

[9] Esquivel, Diego & Valverde, Nicole. (2024). Implementation of holographic displays to increase realism in virtual reality through 3D images that simulate being in the environment. Revista Tecnología en Marcha. Tecnología en Marcha. Vol. 37, special issue. June, 2024. IEEE Latin American Electron Devices Conference (LAEDC). Pág. 24-29.

[10] Ford, John & Merchant, Altaf & Bartier, Anne-Laure & Friedman, Mike. (2018). The cross-cultural scale development process: The case of brand-evoked nostalgia in Belgium and the United States. Journal of Business Research. 83. 10.1016/j.jbusres.2017.09.049.

[11] Gineikiene. Justina & Diamantopoulos, Adamantios)2017("I hate where it comes from but I still buy it: Countervailing influences of animosity and nostalgia," Journal of International Business Studies, Palgrave Macmillan;Academy of International Business, vol. 48(8), pages 992-1008, October.

[12] Gowda.V, Sathyanarayana & H., Archana. (2024). THE ROLE OF BRAND STORYTELLING IN CREATING EMOTIONAL CONNECTIONS. ShodhKosh: Journal of Visual and Performing Arts. 5. 4387-4392. 10.29121/shodhkosh.v5.i1.2024.4576.

[13] Holbrook, M. B., & Schindler, R. M. (2003). Nostalgic bonding: exploring the role of nostalgia in the consumption experience. Journal of Consumer Behaviour, 3(2), 107–127. https://doi.org/10.1002/cb.127.

[14] Kim, I., Kim, W. S., Kim, K., Ansari, M. A., Mehmood, M. Q., Badloe, T., & Rho, J. (2021). Holographic metasurface gas sensors for instantaneous visual alarms. Science Advances, 7(15), eabe9943.

[15] Kumari, Khushi & Trivedi, Nishant. (2025). The Future of Holographic Animation: Applications and Challenges in Advertising, Entertainment, and Education. Conference of New Media, Animation & Visual Narratives in the 21st Century.

[16] Musha, T. (2012). Holographic View of the Brain Memory Mechanism Based on Evanescent Superluminal Photons. Information, 3(3), 344-350. https://doi.org/10.3390/info3030344.

[17] Özhan, Ş., & Talih Akkaya, D. (2020). The Effect of Nostalgia Proneness on Ad-Evoked Nostalgia, Brand Attitude and Purchase Intention. Istanbul Business Research, 49(2), 380-396. https://doi.org/10.26650/ibr.2020.49.0050.

[18] Özkan Pir, Esra. (2019). Nostalgic evolution of marketing: retro marketing. The Journal of Social Science. 10.30520/tjsosci.616780.

[19] Routledge, Clay & Arndt, Jamie & Wildschut, Tim & Sedikides, Constantine & Hart, Claire & Juhl, Jacob & Vingerhoets, Ad & Schlotz, Wolff. (2011). The Past Makes the Present Meaningful: Nostalgia as an Existential Resource. Journal of Personality and Social Psychology. 101. 638-52.

[20] Routledge, Clay & Wildschut, Tim & Sedikides, Constantine & Juhl, Jacob & Arndt, Jamie. (2012). The power of the past: Nostalgia as a meaning-making resource. Memory (Hove, England). 20. 452-60 .

[21] Sadek, Shimaa. (2020). Dynamic Hologram shows as a Digital Advertising Entry for Commercial Centers. 9. 10.21608/idj.2019.83609

[22] Sedikides, C., Wildschut, T., Arndt, J., & Routledge, C. (2008). Nostalgia: Past, Present, and Future. Current Directions in Psychological Science, 17(5), 304-307 .

[23] Shvetsov, Alexey & Alsamhi, Saeed. (2024). When Holographic Communication Meets Metaverse: Applications, Challenges and Future Trends. IEEE Access. PP. 1-1.

[24] Sierra, J.J. and McQuitty, S. (2007) Attitudes and Emotions as Determinants of Nostalgia Purchases: An Application of Social Identity Theory. Journal of Marketing Theory and Practice, 15, 99-112. http://dx.doi.org/10.2753/MTP1069-6679150201

[25] Son, Jung-Young & Lee, Hyoung & Lee, Beom-Ryeol & Lee, Kwang-Hoon. (2017). Holographic and Light-Field Imaging as Future 3-D Displays. Proceedings of the IEEE. PP. 1-16. 10.1109/JPROC.2017.2666538.

[26] Sparrow, R. (2021) Why machines cannot be moral. AI & Soc 36, 685–693.(٢٠٢١)

[27] Steinert, Steffen & Dennis, Matthew. (2022). Emotions and Digital Well-Being: on Social Media's Emotional Affordances. Philosophy & Technology. 35. 10.1007/s13347-022-00530-6.

[28] Tinwell, Angela & Nabi, Debbie & Williams, Andrew. (2011). Facial expression of emotion and perception of the Uncanny Valley in virtual characters. Computers in Human Behavior. 27. 741-749. 10.1016/j.chb.2010.10.018.

[29] Vuković, Dijana & Untersweg, Tanja. (2024). The Current Role of Retro Marketing. MAP Social Sciences. 5. 78-87. 10.53880/2744-2454.2024.5.78.

[30] Wildschut, T., Sedikides, C., Arndt, J. and Routledge, C.D. (2006) Nostalgia: Content, Triggers, Functions. Journal of Personality and Social Psychology, 91, 1-59. http://dx.doi.org/10.1037/0022-3514.91.5.975

[31] Xu, Z., Sun, D., Xia, G., & Wang, S. (2025). Exploring Emotional and Cognitive Engagement with Holographic Displays in Museums. Journal on Computing and Cultural Heritage. https://doi.org/10.1145/3736772.

[32] Yao, Liuye & Lu Zhou, Zhiyu Qian, Qiaoqiao Zhu, Yangyang Liu, Yameng Zhang, Weitao Li, Lidong Xing,(2022) Exploring the impact of 3D movie watching on the brain source activities and energy consumption by ESI and fNIRS, Biomedical Signal Processing and Control, Volume 71, Part B, 2022, 103194,

[33] Zhuang, Ziting. (2023). Nostalgia Marketing: Brand Renewal of "Old Firms" Based on Consumer Emotional Reconstruction——Take the Great White Rabbit Milk Candy as an Example. Highlights in Business, Economics and Management. 23. 904-909. 10.54097/ky3bph60.

Abstract paper – Poster

Holographic Breakdown at GUP-Induced Critical Radius

Sara Motalebi

Department of Physics, School of Sciences, Tarbiat Modares University, P.O.Box 14155-4838, Tehran, Iran.
Email: sara.motalebi@modares.ac.ir

Abstract. We perform a comprehensive analysis of the Generalized Uncertainty Principle (GUP) in Anti-de Sitter space, revealing a fundamental quantum gravity scale. This critical radius governs three interconnected phenomena: (i) holographic breakdown signaled by vanishing boundary stress tensor and (ii) complex central charge c_{eff}, and (iii) Page curve modification through information recovery dynamics ($\Delta S_{\text{recovery}} > 0$). These effects establish a consistency condition for valid AdS/CFT duality. The critical radius emerges as the true Planck scale frontier, where black hole transforms into stringy remnants and information scrambles topologically. It can be interpreted as a black hole-to-string transition point, supported by entropy divergence.

References

[1] F. Scardigli, Phys. Lett. B 452, 39 (1999)

[2] S. Mignemi, Mod. Phys. Lett. A 25, 1697 (2010)

[3] A. Kempf et al., Phys. Rev. D 52, 1108 (1995)

[4] J. Maldacena, Adv. Theor. Math. Phys. 2, 231 (1999)

[5] G. T. Horowitz & J. Polchinski, Phys. Rev. D 55, 6189 (1997)

Proceedings of the 4th International Conference on Holography and its Applications

18 to 19 September, 2025, Khazar University, Baku, Azerbaijan. ICHA4(2025)309

Full paper - Poster

Near- and Far-Field X-ray Holography Simulations of Vibrational Dynamics in Ammonia

F. Allahbakhshi Hafshejani [1], Z. Allahbakhshi Hafshejani [2], P. Nedaei[3], and M. Rezvani Jalal[1]

[1]University of Malayer, Malayer, Iran

Email: fatemeallahbakhshi80@gmail.com

[2]University of Malayer, Malayer, Iran

Email: zahraallahbakhshi80@gmail.com

[3]University of Isfahan, Isfahan, Iran

Email: parsanedaei.2001@gmail.com

Abstract. In this study, we demonstrated an idea of generating atomic-scale hologram of a molecule within one of its vibrational modes using X-ray holography. Hologram is recorded by incident X-ray wave, upon the molecule after triggering one of its vibrational modes. For simplicity, the ammonia (NH3) molecule is chosen as a test molecule while triggered in two distinct vibrational modes: the symmetric stretching and the scissoring modes. The result depicts that the vibrational dynamics modulate the holographic patterns, suggesting the way for developing a new technique of time-resolved molecular holography that captures both atomic position and vibrational state.

1 Introduction

Holographic images of a molecule during vibration in a specific mode, can be used to record dynamical behavior of a molecule under specific circumstances. Capturing this hologram requires the source with wavelength in atomic orders, e.g. XFELs which opens opportunities for imaging at atomic resolution with femtosecond temporal precision [1, 2].

The main idea involves triggering a specific vibrational mode of the target molecule (which in our case is ammonia) by use of tuned IR radiation, then capturing its holographic signature using ultrashort X-ray pulses as source [3]. This approach, allows capturing both static structure and dynamic changes during vibrations.

1.1 X-Ray Holography

Hologram itself, is used to capture both amplitude and phase; considering a wave coming from a target sample, must be captured, in order to achieve this goal, a reference wave must be used to interfere from the one coming from the sample. Due to inference between reference and object wave, a pattern is created which carries information about both the phase and amplitude

of the wave coming from the target sample, hence by capturing interference pattern a recording is created, called hologram.

Now without presence of the original sample, one can reconstruct the information, just by illuminating the hologram obtained from the sample. In simple words, holography means recording and reconstruction of waves [4].

General equation which governs holography, is as follows:

$$I = |R + O|^2 = (R + O)(R + O)^* = |R|^2 + |O|^2 + 2 \cdot \Re(R \cdot O^*) \quad (1)$$

where R and O represent reference and object waves respectively, and I is intensity caused by interference. $\Re$ sign denotes real part operation [4, 5].

X-ray holography on the other hand, is an imaging technique with no need of lenses, that records interference of the reference wave and scattered X-rays from the sample. This technique also allows computationally reconstruction of 3D structural information with no need of optical elements. In addition, resolution beyond visible light limits is achievable [5, 6]. Several applications for X-ray holography are reported in:

Material Science

Atomic Imaging: Mapping of 3D atomic arrangement, e.g., Sr atoms in SrTiO3 [7].

Defect Analysis: Revealing distortions of lattice around dopants, e.g., Mn in GaAs [8].

Dynamics: Capturing nanoparticle explosions by femtosecond pulses [9].

Biology

"Water Window" Imaging: Natural contrast can be provided for hydrated samples, e.g. bacteria Cobetia marina, by soft X-rays (2.48 4.13 nm) [10].

Radiation Therapy: Targeting tumors while sparing healthy tissue [11].

Neural Reconstruction: 3D imaging of neurons at sub-100nm [12].

Industry

Nanomagnetism: Capturing resonant XH images of magnetic domains in Co/Pt films [13].

Battery Electrodes: Quantification of microstructural changes in fuel cells [14].

Another application of X-ray holography is discussed in our study, which can become useful in subjects such as atomic and molecular physics, material science, industry, etc.; hologram of molecular vibrational modes.

1.2 The Ammonia Molecule: Structure and Vibrational Dynamics

Ammonia (NH3), contains 4 atoms, with a pyramid like geometry with nitrogen at the top, bonded to 3 hydrogen atoms, each at other lower corners, forming a molecule with C3v symmetry. Bonds are formed between three free electrons of N in the 2p orbitals, each with one free electron of three H atoms in 1s orbitals. These bonds adopt a geometry with bonding angle of 107.3◦ due to sp3 hybridization, and create a non-planar structure with a permanent dipole moment (~1.5D) directed from N to H plane. Ammonia has a unique feature, inversion motion; N atom can move through the plane of H atoms (bottom surface

of pyramid), switching between two equivalent pyramidal configurations, which leads to a double-well potential with a small energy splitting between the antisymmetric and symmetric vibrational states. Ammonia has six vibrational modes ($3N - 6$ for nonlinear molecules) including symmetric stretch (A1), asymmetric stretch (E), symmetric bending (umbrella mode, A1), and asymmetric bending (scissoring, E). Triggering each mode requires a specific wavelength and polarization, e.g. symmetric stretch mode must be triggered under IR radiation of wavelength $3337cm^{-1}$ and polarization along the molecular symmetry, or asymmetric bending is triggered under IR radiation of wavelength in range $1600\sim1700cm^{-1}$ and linear polarization perpendicular to the NH3 symmetry axis [15].

2 Results and Discussion

We considered three different states of ammonia molecule: without vibration, the symmetric mode, and the scissoring mode, then simulated hologram for each of them in both near-field and far-field. By investigating the holograms captured at the near-field region (figure 1), the results show containing fluctuating pattern within capturing, consequently information obtained are not clear enough to become useful.

On the other hand, holograms captured at far-field region (figure 2), present more clarity about the effects of vibration on resulted hologram. However, it is not hard to recognize that the far-field holograms are similar to their near-field correspondents except the fluctuating pattern overlap is removed.

By comparing the pattern generated in relaxed state (no vibration) with other two patterns, it can be seen how vibrations modulate the holographic patterns; in a specific vibrational mode, the atom which does not involve any movements, will cast a shadow, e.g. in the symmetric mode (figure 2b) nitrogen atom at center, is fixed at its position while other three hydrogen atoms obey periodic movement toward and away from it, following sinusoidal path which indeed washes out the shadow.

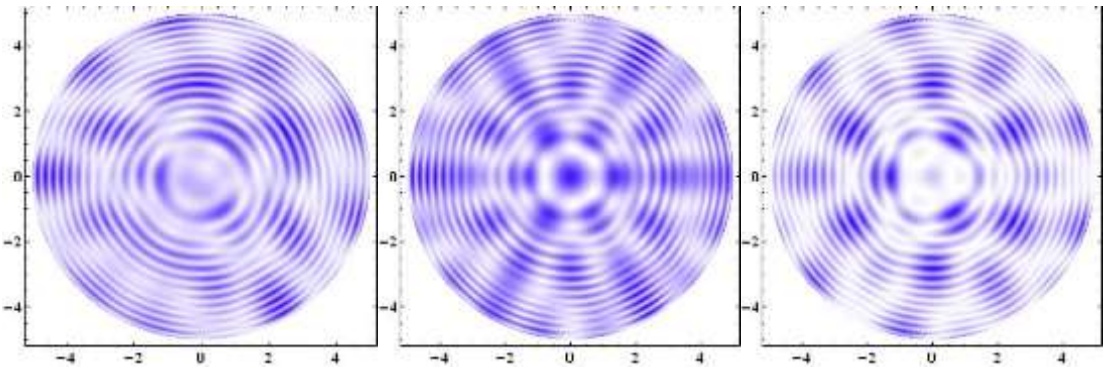

(a) (b) (c)

Figure 1: Holograms captured at near-field region: (a) without vibration, (b) symmetric mode, and (c) scissoring mode (axes units are micro-meter)

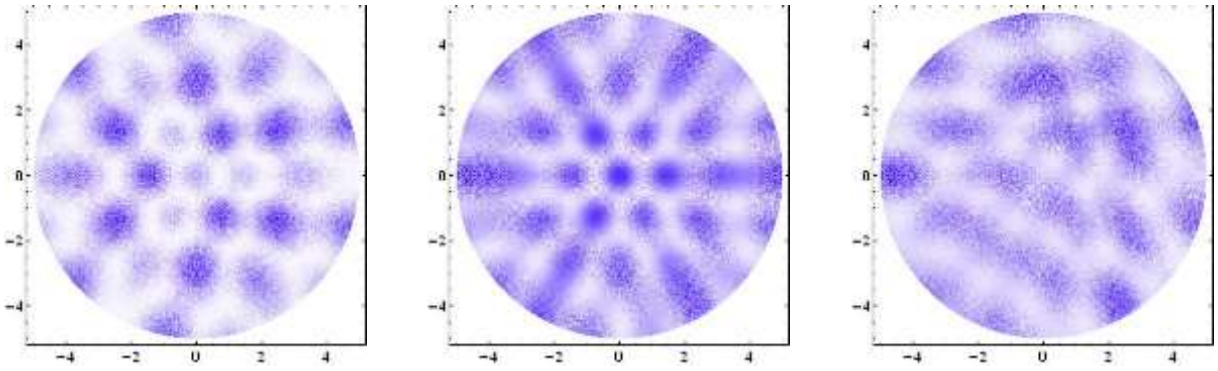

(a) (b) (c)

Figure 2: Holograms captured at far-field region: (a) without vibration, (b) symmetric mode, and (c) scissoring mode (axes units are centi-meter)

In other words, shadows correspond to the atoms which are staying still while the bright areas belong to the atoms which are pivoting.

Another observation in captured hologram, is white grains in far-field holography patterns, even by increasing number of points in simulation, white grains are not removed, therefore it is predicted, grains are caused by speckle-gram of illumination source.

3 Conclusion

Capturing holographic image of a dynamic system such as vibrating molecule, helps to understand both dynamic and static behaviors of the system in question. Holographic pattern generated by impacts of motion, is the modulated form of pattern generated while the system is in relaxed situation, consequently this modulation arise by work of the parts in system which stay still together with the parts which are following specific path of motion.

For future works, there are two topics to be studied: analysis of white grains appeared in far-field hologram and how to reconstruct the captured hologram.

References

[1] Henry N. Chapman. X-ray free-electron lasers for the structure and dynamics of macro-molecules. Annual Review of Biochemistry, 80:381–401, 2011.

[2] Richard Neutze, Remco Wouts, David van der Spoel, Edgar Weckert, and Janos Hajdu. Po-tential for biomolecular imaging with femtosecond x-ray pulses. Nature, 406(6797):752– 757, 2000.

[3] S. S. Alimpiev, N. V. Karlov, A. M. Prokhorov, B. G. Sartakov, E. M. Khokhlov, and A. L. Shtarke. Investigation of vibrationally excited ammonium molecules by the ir-uv resonance method. Soviet Physics JETP, 41(5):871–877, 1975.

[4] B.E.A. Saleh and M.C. Teich. Fundamentals of Photonics. Wiley Series in Pure and Applied Optics.

[5] MR Howells and CJ Jacobsen. X-ray holography. Synchrotron Radiation News, 3(4):23– 28, 1990.

[6] Bingjun Shi, Yuan Fu, and Yan Yang. Applications of x-ray holography. International Journal of Optics, 2021(1):7711028, 2021.

[7] Miklo´s Tegze, Gyula Faigel, Stefano Marchesini, Michel Belakhovsky, and Olivier Ulrich. Imaging light atoms by x-ray holography. Nature, 407(6803):38–40, 2000.

[8] M Kopecky`, J Kub, E Busetto, A Lausi, M Cukr, V Nova´k, K Olejn´ık, JP Wright, and J Fa´bry. Location of mn sites in ferromagnetic ga1- xmnxas studied by means of x-ray diffuse scattering holography. Applied Crystallography, 39(5):735–738, 2006.

[9] Henry N Chapman, Stefan P Hau-Riege, Michael J Bogan, Sasˇa Bajt, Anton Barty, Se´bastien Boutet, Stefano Marchesini, Matthias Frank, Bruce W Woods, W Henry Benner, et al. Femtosecond time-delay x-ray holography. Nature, 448(7154):676–679, 2007.

[10] Thomas Gorniak, R Heine, Adrian Paul Mancuso, Florian Staier, Christof Christophis, ME Pettitt, A Sakdinawat, R Treusch, N Guerassimova, J Feldhaus, et al. X-ray holo- graphic microscopy with zone plates applied to biological samples in the water win- dow using 3rd harmonic radiation from the free-electron laser flash. Optics express, 19(12):11059–11070, 2011.

[11] Habib Madjidi-Zolbin and Saeed Jafari. Cancer treatment by x-ray holography. In Lasers in Medicine and Dentistry: Diagnostics and Treatment, volume 2887, pages 84–90. SPIE, 1996.

[12] Aaron T Kuan. Dense neuronal reconstruction through x-ray holographic nano- tomography. Biophysical Journal, 118(3):290a, 2020.

[13] S. Streit-Nierobisch, D. Stickler, C Gutt, L-M Stadler, H Stillrich, C Menk, R Fro¨mter, C Tieg, O Leupold, HP Oepen, et al. Magnetic soft x-ray holography study of focused ion beam-patterned co/pt multilayers. Journal of Applied Physics, 106(8), 2009.

[14] Julie Villanova, Je´roˆme Laurencin, Peter Cloetens, Pierre Bleuet, Ge´rard Delette, Heikki Suhonen, and Franc¸ois Usseglio-Viretta. 3d phase mapping of solid oxide fuel cell ysz/ni cermet at the nanoscale by holographic x-ray nanotomography. Journal of Power Sources, 243:841–849, 2013.

[15] Wolfgang Demtro¨der. Atoms, Molecules and Photons: An Introduction to Atomic-, Molecular- and Quantum Physics. Springer, 3 editions, 2019

Full paper - Poster

Reconstruction of Far-Field Holograms of Ammonia Vibrational Modes

Z. Allahbakhshi Hafshejani[1], F. Allahbakhshi Hafshejani[2], P. Nedaei[3], M. Rezvani Jalal[1]
[1] University of Malayer, Malayer, Iran.
Email: zahraallahbakhshi80@gmail.com
[2] University of Malayer, Malayer, Iran.
Email: fatemeallahbakhshi80@gmail.com
[3] University of Isfahan, Isfahan, Iran.
Email: parsanedaei.2001@gmail.com

Abstract. In this study we present a reconstruction of far-field X-ray hologram of a vibrating ammonia (NH_3) molecule. On previously simulated holograms of relaxed state and vibrational states symmetric-stretch and scissoring, we demonstrated the importance of holography for molecular analysis in vibrational behavior. Here we reversed the approach; given a hologram of specific vibrational mode, and reconstructing recorded information. This will enable studying vibrational behavior even if the molecule in question is not presented.

1 Introduction

Holography enables recording of both amplitude and phase information [1], when a wave encounters target it undergoes scattering and each of the points on the target in question responsible of scattering, is considered as secondary sources, and by encoding interference pattern of these waves with a reference beam, both amplitude and phase information can be recorded.

X-ray holography, have some special properties like lensless imaging at atomic scale when using short-wavelength sources such as X-ray free-electron lasers (XFELs) [2]. In previous work [3], we demonstrated near- and far-field holograms of an ammonia in three different states:
(i) relaxed state, when none of vibrational modes are triggered and the molecule remains static without dynamic variations, (ii) symmetric-stretch when all three hydrogen atoms move forward and backward along a sinusoidal path getting close and far from nitrogen, and (iii) scissoring mode when only of three hydrogen atoms remains static and other two atoms undergo dynamical variations.

By analyzing recorded holograms, we figured that far-field holograms provide more accurate information based on static behavior and dynamic variations [4]. While having a holographic image of a target, several information can be resolved from the hologram about the target, e.g. geometrical shape and dynamical variations.

In this paper we demonstrate reconstructed information from the holographic recordings described in previous work by presenting a comprehensive computational framework that connects far-field holographic imaging with vibrational mode molecular dynamics. Our approach involves following steps in order to reconstruct the captured holographic image in our previous work [3]:

1. modeling ammonia molecule as a four-body spring-mass system [5],
2. solving for normal modes and computing time-dependent positions during oscillation [6],
3. calculating wave scattering from the oscillating molecular system [7],
4. implementing holographic reconstruction algorithms [8],

to recover molecular structure and dynamics from simulated interference patterns.

2 Theory and Background

By examination of equations on recorded intensity as hologram and applying inverse mathematics, it is possible to achieve information stored on holographic image, therefore it is necessary to understand forward path of holography in order to figure out the backward path.

2.1 Hologram Reconstruction

The recorded hologram intensity is:

$$I(\mathbf{r}) = |R(\mathbf{r}) + O(\mathbf{r})|^2 = |R|^2 + |O|^2 + 2\Re(R \cdot O^*) \tag{1}$$

where R is the reference wave, O the object wave, both at plane of detector, and the sign $\Re(\cdot)$ denoted real-part. This expression is identical to the one described in previous paper. There are two regimes of reconstruction based on the regions of recorded hologram, (i) far-field (Fraunhofer) regime and (ii) near-field (Fresnel) regime [8].

(i) Far-field (Fraunhofer) reconstruction Consider a detector is placed in a large distance compared to the dimensions of system, the object wave $O(\mathbf{r})$ at the detector is proportional to the Fourier transform of the object exit wave $o(\rho)$ in the sample plane:

$$O(\mathbf{q}) \propto F[o(\rho)](\mathbf{q}), \qquad \boldsymbol{q} = \frac{2\pi}{\lambda z}\boldsymbol{r} \tag{2}$$

and reconstruction reduces to retrieving $o(\rho)$ by inverse Fourier transform of the measured complex amplitude or by applying phase-retrieval when only intensities are measured.

(ii) Near-field (Fresnel) reconstruction For propagation distances not so far to satisfy the conditions required to be in Fraunhofer region, the Fresnel diffraction integral governs free-space propagation. We implement back-propagation by convolution with the Fresnel kernel that can be converted to multiplication in Fourier domain:

$$o(\rho) = F^{-1}[F[O(\mathbf{r})](\mathbf{k})H_{\text{Fresnel}}(\mathbf{k})], \qquad H_{\text{Fresnel}}(\mathbf{k}) = e^{-i\frac{\lambda z}{4\pi}|\mathbf{k}|^2} \qquad (3)$$

3 Methodology

We present a simple physical framework in order to reconstruct the vibrational state of a molecule from a single recorded hologram. The method involves molecular dynamics, coherent scattering theory, and analytical time-averaging to relate the measured holographic intensity pattern to the instantaneous atomic motion.

3.1 Molecular Representation and Vibrational Modeling

The configuration used is spring-mass model, i.e. the molecule is considered as a set of point masses (atoms) connected by springs (chemical bonds). Based on the molecular geometry, equilibrium positions are determined, and bond stiffnesses are approximated via uniform spring constant.

The vibrational eigenmodes are obtained by solving the coupled equations of motion in matrix form, yielding discrete eigenfrequencies and mode shapes. As a general rule of thumb, any instantaneous molecular configuration can be expressed as a superposition of these modes with given amplitude and phases.

3.2 Scattering from Vibrating Atoms

Incident coherent wave (X-ray laser) is considered a plane wave, and when encounters the molecule in question (ammonia), each atom acts as a point scatterer, i.e. they become secondary sources of emission, re-emitting spherical waves with phases depended on their instantaneous positions.

Consequently, when the molecule in question, has vibrations, these motions modulate the incident plane wave coming from the source, and by encoding interference pattern of secondary waves with a reference wave, dynamical variations of the molecule is recorded. As mentioned in previous paper, simulations show when an atom is in motion, compared to relaxed state, it casts no shadows, i.e. pivoting behavior of atoms, washes out cast shadows in relaxed state and leave bright spots instead. Analytical time-averaging over the exposure duration yields scattering amplitudes weighted by Bessel functions, analogous to a generalized Debye-Waller factor. This formulation captures the redistribution of scattered intensity due to molecular motion without requiring time-resolved measurements.

3.3 Hologram Formation and Time-Averaged Intensity

The hologram is a recording of interference pattern generated by superposition of a reference wave (unscattered) and an object wave (scattered). In the case, which the object in question (in our case the ammonia) has dynamic behavior, generated pattern corresponds to the time- averaged intensity

distribution over many oscillation periods. This averaging encodes mode- specific signature in the interference pattern rather than just blurring, i.e. the resulted capturing contains both static structure and dynamic behavior.

4 Results and Discussion

In reconstruction process from recorded holograms in previous paper, for (i) relaxed state, (ii) symmetric stretch mode, and (iii) scissoring mode, two results are illustrated for each:

1. 1D hologram
2. Real static structure and vibrational state

By presenting and describing each case, we break through the topic in more detailed manner.

4.1 Relaxed State

In relaxed state, no dynamic behavior is observed and this case can be used as reference state in order to compare the effect of motion on holographic imaging. Figure 1 shows 1D-holographic image of relaxed state, this hologram is generated by considering the cross-section of imaging system, like the case of analyzing resulted interference pattern from Young's double-slit experiment from the side view which is $sinc$ function. All other 1D-holograms in forward sections follow this description. Figure 2 by comparing both images, shows that in static situation all four atoms in ammonia molecule are casting shadows on screen, in which the shadow resulted from nitrogen molecule is darker and has smaller spot size than the shadows cast from hydrogen atoms, because of the difference in their atomic sizes. Also, by using relaxed state as reference image, one can tell in other images, darker shadow spots are defining position of nitrogen atom while the brighter shadow spots are defining positions for hydrogen atom.

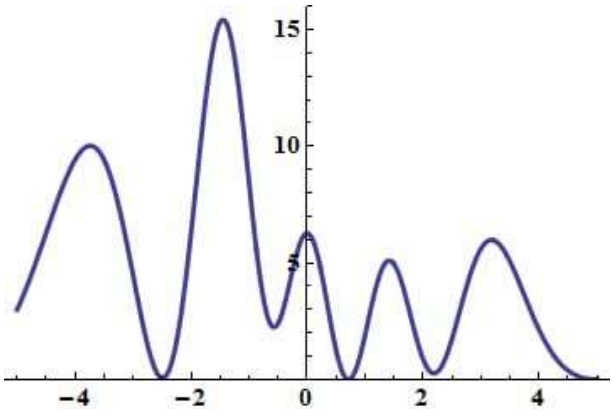

Figure 1. 1D hologram of relaxed state (axes units are in cm)

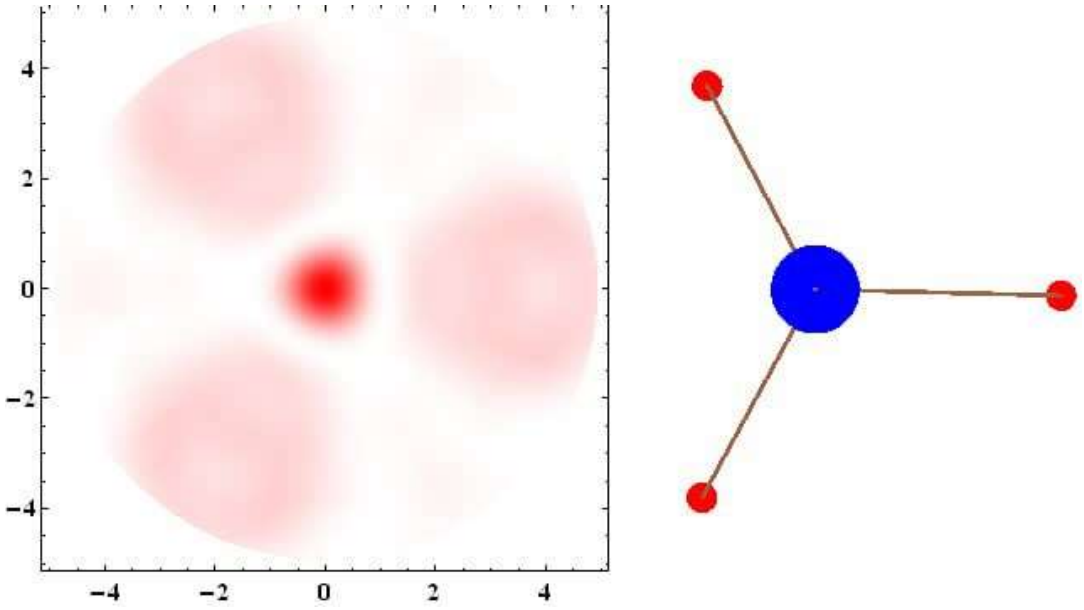

Figure 2. Recontructed moleculare structure from hologram (axes units in left plot are in **Å**)

4.2 Symmetric Stretch

In the case of symmetric stretch mode, all hydrogen atoms have motion. By comparing resulted images with previous figures, it shows that the movement of hydrogen atoms lead to disappear-ance of cast shadows by them. Also, the symmetricity can be observed from both images in (figure 3); It can be seen from (figure 3a) that symmetric motion of hydrogen atoms with respect to central nitrogen atom lead to more symmetricity compared with (figure 1). In addition by comparison of (figure 2) and (figure 3b), one can observe that cast shadow from nitrogen remains unchanged because it is still fixed at its position will disruption in shadow spots around it is symmetric.

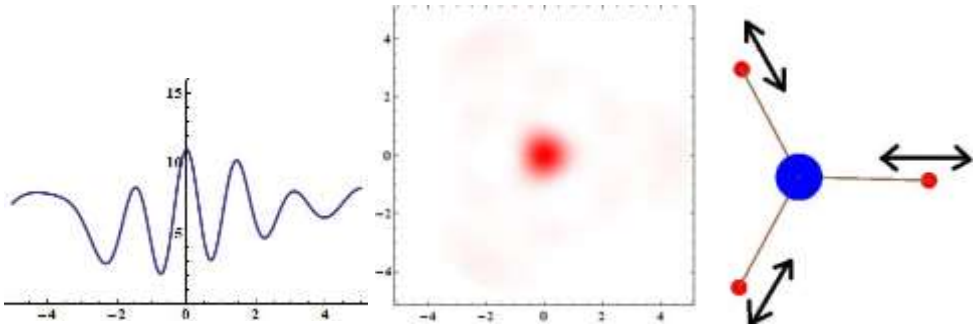

3.3.1 1D-hologram (axes units are in *cm*)

3.3.2 Recontructed moleculare structure from hologram (axes units in left plot are in **Å**)

Figure 3. Hologram reconstruction for symmetric stretch vibrational mode of ammonia

4.3 Scissoring Mode

Now at last, for the case of scissoring mode, in which only on of three hydrogen atoms remain fixed at its position while other two are under motion, it can be seen from (figure 4) that the effect of movement on holographic images is similar to previous cases. Therefore, in order to reconstruct the molecular state from captured hologram we must first consider again that motion is the main reason of cast shadow disruption compared with relaxed state. By comparing (figure 4a) and (figure 1), effective change can be observed in the right side of $y - axis$ while it corresponds to moving hydrogen atoms. Also, by a comparison between (figure 2), (figure 3b), and (figure 4b), differences are easy to identify; Whenever an atom remains fixed in its position, cast shadows still unchanged, in contrast, any movement leads to disruption in cast shadow with respect to the reference (relaxed state).

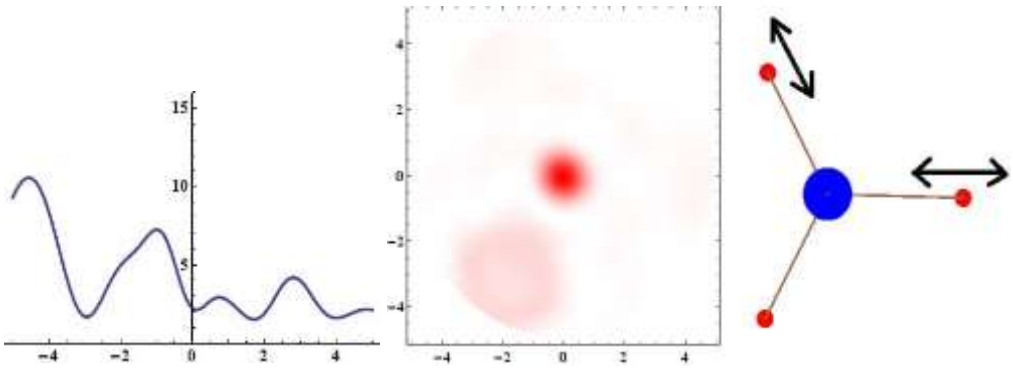

Figure 4. Hologram reconstruction for scissoring vibrational mode of ammonia

1D-hologram (axes units are in *cm*)

Recontructed moleculare structure from hologram (axes units in left plot are in **Å**)

5 Conclusion

Holographic reconstruction of ammonia in relaxed state and two distinct vibrational modes, symmetric stretch and scissoring, reveals two major information: (i) atomic motions are the reasons behind disruptions in interference pattern and (ii) structure geometry and current state of vibration can be shown and analyzed by hologram of the molecule with no necessary need of molecule presence. The relaxed state provides a perfect reference and enables the possibility of predictions about molecule dynamics in question when it chooses the dynamic states instead of remaining static. In addition, comparing each mode to the static reference enables direct identification of vibrational dynamics from a single hologram which confirms that the method is effective for structural and dynamic analysis.

References

[1] Dennis Gabor. A new microscopic principle. Nature, 161(4098):777–778, 1948.

[2] Henry N Chapman, Petra Fromme, Anton Barty, et al. Femtosecond x-ray protein nanocrystallography. Nature, 470:73–77, 2011.

[3] Allahbakhshi Hafshejani F., Allahbakhshi Hafshejani Z., Nedaei P., Rezvani Jalal M., Near- and far-field x-ray holography simulations of vibrational dynamics in ammonia. 2025.

[4] Joseph W Goodman. Introduction to Fourier Optics. Roberts and Company Publishers, 2005.

[5] Wolfgang Demtro¨der. Atoms, Molecules and Photons: An Introduction to Atomic-, Molecular- and Quantum Physics. Springer, Berlin, Heidelberg, 2nd edition, 2010.

[6] Herbert Goldstein, Charles Poole, and John Safko. Classical Mechanics. Addison Wesley, 3rd edition, 2002.

[7] Max Born and Emil Wolf. Principles of Optics. Cambridge University Press, 7th edition, 1999.

[8] Bahaa E. A. Saleh and Malvin Carl Teich. Fundamentals of Photonics. Wiley, Hoboken, NJ, 3rd edition, 2019.

Proceedings of the 4th International Conference on Holography and its Applications

18 to 19 September, 2025, Khazar University, Baku, Azerbaijan. ICHA4(2025)311

Generation of Perfect Vortex Beam Arrays Using Axicon Embedded in Singular Almost Periodic Phase Structures

Mohsen Samadzadeh[1], Saifollah Rasouli[1,2], Davud Hebri [3]
[1]Department of Physics, Institute for Advanced Studies in Basic Sciences (IASBS), Zanjan. Iran
Email: mohsam@iasbs.ac.ir
[2]Center for International Scientific Studies and Collaboration (CISSC), Ministry of Science, Research and Technology, Tehran.
Email: rasouli@iasbs.ac.ir
[3]Department of Physics and Atmospheric Science, Dalhousie University, Halifax, Nova Scotia B3H 4R2, Canada
Email: davud.hebri@iasbs.ac.ir

Abstract. In this work, we present an experimental method for generating circular arrays of Perfect Vortex Beams (PVBs). The arrays, featuring distinct topological charges, are produced using an axicon embedded within singular almost-periodic phase structures (SAPPSs). A Fourier lens transforms an incident Gaussian beam modulated by the SAPPS, resulting in an array of PVBs at the focal plane. Such structured PVB arrays hold significant potential for applications across various scientific and research domains, including optical trapping, parallel particle manipulation, and structured light-matter interactions.

1 Introduction

Optical vortices are a class of structured light fields characterized by a helical phase structure of the form $\exp(jl\phi)$, where ϕ denotes the azimuthal coordinate and l represents the topological charge (TC). This phase structure imparts an orbital angular momentum (OAM) of $l\hbar$ per photon, where $\hbar$ is the reduced Planck constant [1]. The ability of vortex beams to carry and transfer angular momentum to matter has made them highly valuable in a wide range of optical systems.

Among the most commonly studied optical vortex beams are Laguerre-Gaussian (LG) [2], Bessel-Gaussian (BG) [3-4], and Perfect Vortex Beams (PVBs) [5], each exhibiting unique spatial and propagation properties. For LG and BG beams, both the transverse mode profile and the radius of peak intensity depend on the topological charge l; as l increases, the beam's ring size typically broadens. This intrinsic dependence poses challenges for applications requiring uniform beam size regardless of TC [6].

Perfect vortex beams (PVBs), in contrast, maintain a constant ring radius independent of the topological charge, making them particularly attractive for applications requiring mode uniformity [7]. The ability to generate and control structured arrays of such beams with varying topological charges is crucial for advanced optical applications including high-resolution microscopy[8-9], optical trapping and manipulation [10], quantum entanglement [11], and high-capacity communication systems [12-13].

Recent investigations have explored vortex beam arrays produced through the far-field diffraction of pure amplitude 2N-gonal almost-periodic structures (APSs) illuminated by vortex beams of varying TCs [14]. Additionally, the generation of Bessel beam arrays using axicons embedded in APSs has been demonstrated. Building on these developments, the present study introduces a method for generating arrays of perfect vortex beams using an axicon integrated within singular almost-periodic phase structures (SAPPSs), offering a promising platform for advancing structured light technologies in both classical and

quantum regimes.

Consider a single-ring-spectrum APS as detailed in the appendix of [15]. This optical component was employed for 3D multi-particle trapping in [16]. Here, the impulses are positioned at both the center and the vertices of an octagon in the spectral domain. Building upon this idea, a novel APS can be designed where spectral impulses are located at the center and vertices of a regular polygon [14].

According to the general theory of diffraction, the transmittance function of an SAPPS can be expressed in a generic vector form as:

$$t_{SAPPS}(\mathbf{r}) = \frac{1}{2N}\sum_{n=0}^{N}\cos(2\pi \mathbf{f_n}.\mathbf{r})e^{-i2\pi\frac{r}{r_0}+il\varphi}. \qquad (1)$$

Here we have $\mathbf{f_n} = (\nu\cos\varphi_n, \nu\sin\varphi_n)$ where $\varphi_n = (n-1)\pi/N$ and ν represents the fundamental spatial frequency of the structure. Although the structure defined by equation (1) is not generally periodic, we can define a characteristic fundamental quasi-period for the structure as $\Lambda = \nu^{-1}$. To enable a direct comparison with the general form of APSs in equation [14], we can rewrite equation (1) as:

$$t_{SAPPS}(\mathbf{r}) = \frac{1}{2} + \frac{1}{4N}\sum_{n=1}^{2N}\exp(i2\pi \mathbf{f_n}.\mathbf{r}), \qquad (2)$$

where we used $\mathbf{f}_{N+m} = -\mathbf{f}_m$ for m = 1, 2, ..., N as a result of $\varphi_{N+m} = \varphi_m + \pi$, so that $t_0 = 1/2$, $t_n = (4N)^{-1}$ for $1 \leqslant n \leqslant 2N$, and $t_n = 0$ otherwise.

The optical field immediately after the structure reads:

$$\Psi(\mathbf{r},0) = u(\mathbf{r},0)t_{SAPPS}(\mathbf{r}), \qquad (3)$$

where, in polar coordinates, the field of a Gaussian beam at $u(\mathbf{r},0)$ can be expressed as

$$u(\mathbf{r},0) = \frac{2r^2}{\omega_0^2}e^{\frac{r^2}{\omega_0^2}}. \qquad (4)$$

Upon propagation over the distance z in free space, the field is well known to remain shape-invariant such that

$$u_G(\mathbf{r},z) \propto g(z)e^{\frac{ikr^2}{2q(z)}}\left(\frac{2r^2}{\omega^2(z)}\right), \qquad (5)$$

where g(z), q(z), and w(z) have been defined in Eq. (4) of Ref [14].

Let a Gaussian beam with its waist at z = 0 illuminate an SAPPS. The amplitude of a diffracted wave in focal lens can now be written as:

$$\psi(\mathbf{r},z) = F\left[\frac{1}{2}u_G(r,z) + \frac{e^{-i2\pi(\frac{z}{z_T}+\frac{r}{r_0}\cdot\frac{l\varphi}{2})}}{4N}\sum_{n=1}^{2N}e^{i2\pi\nu r\cos(\theta-\varphi_n)}u_G(r_n,z)\right]. \qquad (6)$$

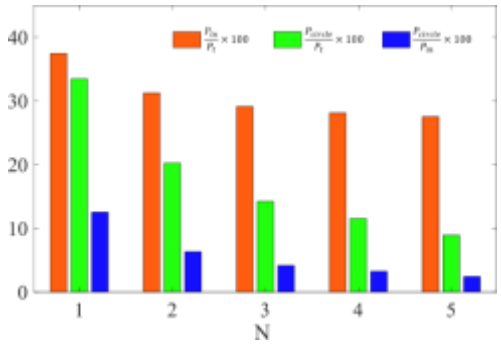

Figure 1: Theoretical comparison of power distribution ratios in SAPPSs for varying N (1 to 5). Power transmittance of the SAPPS versus N (orange bars). The distribution of total impulse along a concentric circle, expressed as a fraction of the transmitted power (green bars) and the incident power (blue bars).

In figure 1 we show the transmitted power as function of N. As is apparent, the power transmission

coefficient decreases with N, approaching 25%. We separate the transmitted power into two parts: P_0, associated with the zero diffraction order or impulse, and P_{circle}, representing the total power of other impulses along a concentric circle.

We show that the power fractions of the zero-order impulse and the higher-order components, relative to the transmitted power, are given by $P_0/P_t = 2N/(2N + 1)$ and $P_{circle}/P_t = 1/(2N + 1)$, respectively. Moreover, their corresponding fractions with respect to the incident power are $P_0/P_{in} = 1/4$ and $Pcircle/P_{in} = 1/(8N)$.

Figures 2 and 3 illustrate the conceptual framework and optical design used for generating PVB arrays with different TCs. As shown in Fig. 2(a), the generation of a single PVB begins with a Gaussian beam that is transformed into a Bessel beam using a spiral phase element. This intermediate Bessel beam is then Fourier transformed by a lens to produce a PVB at its focal plane. The concept is extended in Figure 2(b) to create a PVB array by replacing the spiral phase element with a combination of an axicon and an SAPPS. This configuration generates a Bessel beam array, which is subsequently converted into an array of PVBs through Fourier transformation.

Figure 2 presents the schematic procedure for designing the phase masks required to generate these PVB arrays with controllable and distinct TCs.

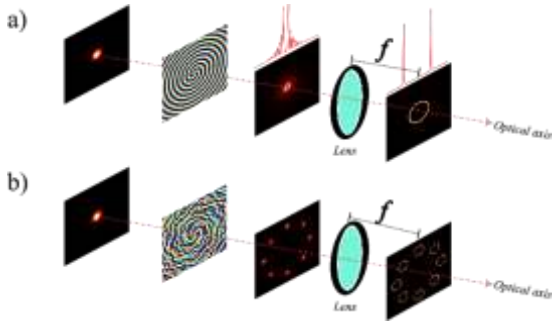

Figure 2 (a) Schematic of PVB generation: a Gaussian beam is converted into a Bessel beam using a spiral phase element, and then transformed into a PVB at the focal plane of a Fourier lens. (b) Extension to a PVB array: the Gaussian beam passes through a combination of an axicon and SAPPS, forming a Bessel beam array, which is then Fourier transformed by a lens into a PVB array.

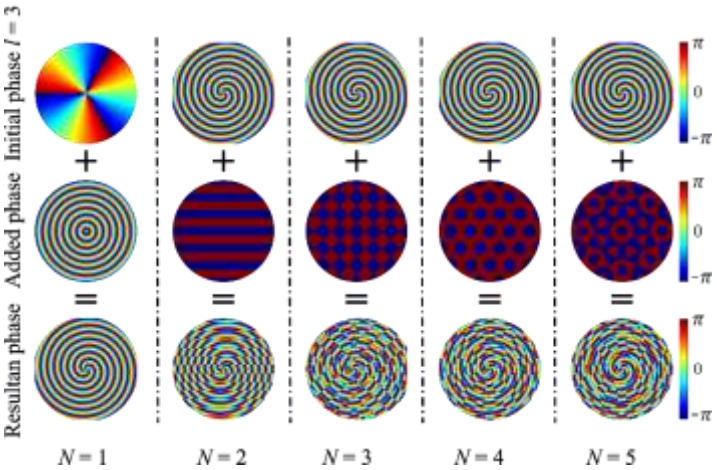

Figure 3. Schematic illustration of the design process for phase masks used to generate PVB arrays with varying TCs.

The experimental setup is shown in Figure 4. A laser beam, after passing through a spatial filter to remove spatial noise originating from the laser source, is collimated using lens L1 and directed onto a spatial light modulator (SLM). Two half-wave plates (λ/2) are placed before and after the SLM to enhance contrast and suppress unwanted noise.

The desired phase pattern is generated by a computer and applied to the SLM, thereby modulating the phase

of the incoming beam. By performing a Fourier transform of the SLM's zero-order diffraction using lens L2, an array of PVBs is formed at the focal plane of the lens, corresponding to the imposed phase pattern. This PVB array is then captured using a CCD camera.

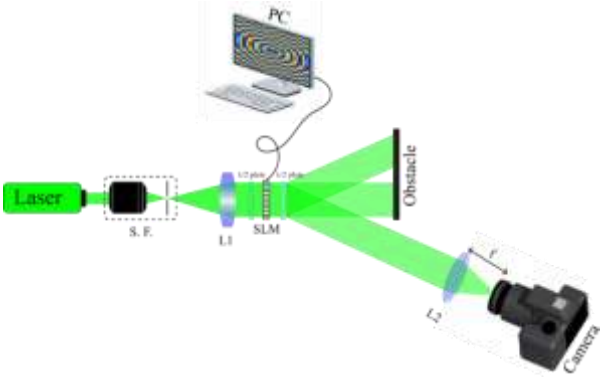

Figure 4. Experimental setup for generating arrays of PVBs. A laser beam is spatially filtered to remove noise, collimated by lens L1, and directed onto a spatial light modulator (SLM). Two half-wave plates (λ/2) placed before and after the SLM optimize polarization for improved phase contrast and noise suppression. The computer-generated phase pattern is applied via the SLM to modulate the beam's phase. A Fourier transform performed by lens L2 forms the PVB array at its focal plane, which is recorded by a CCD camera.

In Figure 5, the first row shows the phase patterns applied to the SLM for N = 1, 2, 3, 4. The second and third rows display the corresponding simulated and experimental results, respectively, of the Fourier transform of the far-field diffraction from these phase patterns, captured at the focal plane of lens L2. In all cases, the topological charge is set to zero, and the radial scaling parameter is fixed at 0.5 mm.

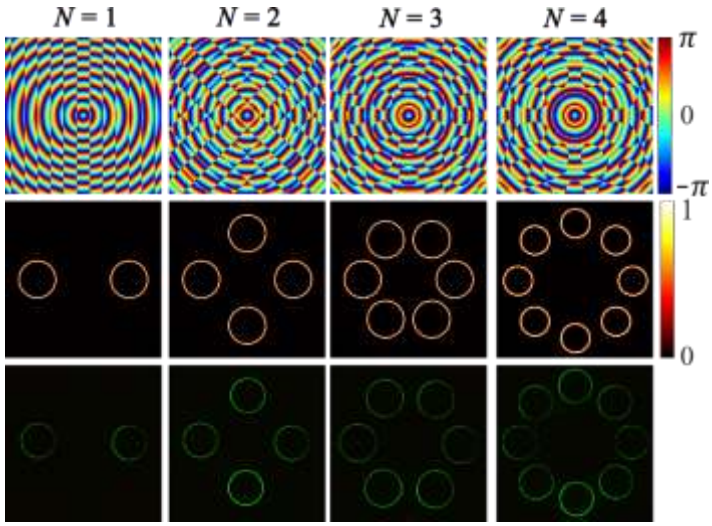

Figure 5. Generation of PVB arrays using SAPPSs with different symmetry orders. Top row: phase masks applied to the SLM for N = 1, 2, 3, 4. Middle row: simulated intensity distributions obtained by Fourier transforming the far-field diffraction of the phase-modulated beams. Bottom row: corresponding experimental results recorded at the focal plane of lens L2. All cases correspond to a topological charge of zero and a fixed radial scaling parameter of 0.5 mm.

In Figure 6, the first and second rows show the simulated and experimental results, respectively, for the PVB array corresponding to N = 2. The first to fourth columns present the results for radial scaling parameters of 0.7 mm, 1 mm, 1.5 mm, and 2 mm, respectively. The results demonstrate that by adjusting the radial scaling parameter, the thickness and diameter of each PVB within the array can be effectively controlled.

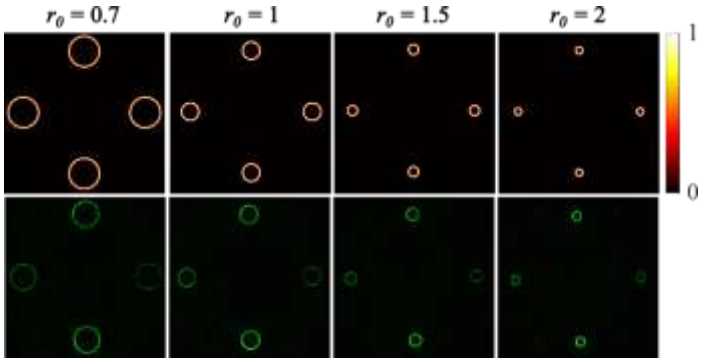

Figure 6. Effect of the radial scaling parameter on the structure of PVB arrays for N = 2. Top row: simulated intensity distributions. Bottom row: corresponding experimental results. Columns from left to right correspond to radial scaling parameters of 0.7 mm, 1 mm, 1.5 mm, and 2 mm, respectively. The results indicate that the beam thickness and diameter of each PVB in the array can be tuned by varying the radial scaling parameter.

In Figure 7, the first row shows the phase patterns applied to the SLM for N = 1, 2, 3, 4. The second and third rows present the simulated and experimental results, respectively, of the Fourier transform of the far-field diffraction from these phase patterns at the focal plane of lens L2. The topological charge values for the phase structures in the first, second, and third columns are 0, 1, and 3, respectively, while the radial scaling parameter is fixed at 1 mm. Both experimental and simulation results indicate that variations in the topological charge do not affect the diameter of the PVBs.

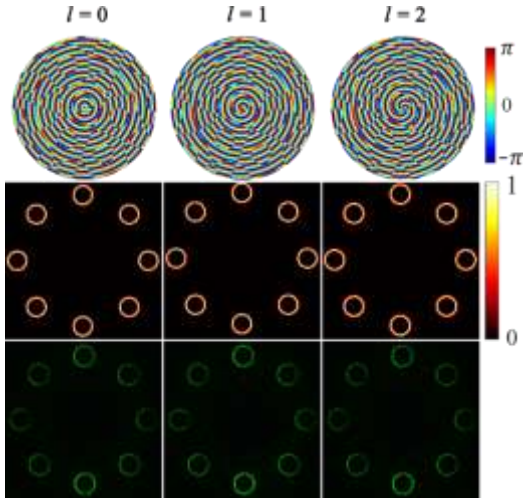

Figure 7. Influence of topological charge on PVB arrays for different symmetry orders N = 1, 2, 3, 4. Top row: phase masks applied to the SLM. Middle row: simulated intensity distributions from the Fourier transform of the modulated beams. Bottom row: corresponding experimental results recorded at the focal plane of lens L2. The topological charges for the phase structures in the first, second, and third columns are 0, 1, and 3, respectively, with a fixed radial scaling parameter of 1 mm. The results show that changing the topological charge does not affect the beam diameter.

Conclusion

In summary, we have demonstrated an effective experimental approach for generating circular arrays of PVBs using an axicon embedded within SAPPSs. By modulating a Gaussian beam with tailored phase patterns and applying Fourier transformation through a lens, we successfully produced structured PVB arrays with controllable topological charges and beam profiles.

Our results confirm that the radial scaling parameter directly influences the diameter and ring thickness of

the PVBs, while the topological charge affects the internal phase structure without altering the beam size. The close agreement between simulation and experimental results validates the robustness and flexibility of the proposed method.
This work offers a versatile platform for creating structured light fields and paves the way for applications in optical manipulation, high-resolution imaging, parallel beam shaping, and light–matter interaction studies where control over beam topology and geometry is essential.

Acknowledgement

This study was supported by the Institute for Advanced Studies in Basic Sciences (No. G2025IASBS12632) and Center for International Scientific Studies and Collaboration (CISSC) of Iran (No. 4020667).

References

[1] L. Allen, M. Beijersbergen, R. Spreeuw, and J. Woerdman, "Orbital angular momentum of light and the transformation of Laguerre-Gaussian laser modes," *Phys. Rev. A*, vol. 45, no. 11, p. 8185, 1992.

[2] J. Y. Bae, Y. G. Kim, H. W. Lee, J. H. Sung, and C. M. Kim, "Generation of low-order Laguerre-Gaussian beams using hybrid-machined reflective spiral phase plates for intense laser-plasma interactions," *Results Phys.*, vol. 19, p. 103499, 2020.

[3] T. Yu, Y. Ma, P. Zhou, H. Zhang, and L. Si, "The generation and verification of Bessel-Gaussian beam based on coherent beam combining," *Results Phys.*, vol. 16, p. 102872, 2020.

[4] C. Lyu, Y. Li, S. Wang, and Y. Wang, "Generation of diffraction-free Bessel beams based on combined axicons," *Opt. Laser Technol.*, vol. 164, p. 109548, 2023.

[5] X. Li, Q. Zhao, P. Zhang, L. Wang, and B. Gu, "Controllable mode transformation in perfect optical vortices," *Opt. Express*, vol. 26, no. 2, pp. 651–662, 2018.

[6] H. Yan, Z. Wang, Y. Li, J. Wang, and Y. Zhang, "Free-space propagation of guided optical vortices excited in an annular core fiber," *Opt. Express*, vol. 20, no. 16, pp. 17904–17915, 2012.

[7] X. Tao, Y. Li, H. Wang, and C. Xie, "Generation of perfect vortex beams with complete control over the ring radius and ring width," *Photonics*, vol. 10, no. 12, 2023.

[8] I. Heller, G. Sitters, O. D. Broekmans, C. Schäffer, and E. J. G. Peterman, "STED nanoscopy combined with optical tweezers reveals protein dynamics on densely covered DNA," *Nat. Methods*, vol. 10, no. 9, pp. 910–916, 2013.

[9] X. Qiu, F. Li, W. Zhang, Z. Zhu, and L. Chen, "Spiral phase contrast imaging in nonlinear optics: seeing phase objects using invisible illumination," *Optica*, vol. 5, no. 2, pp. 208–212, 2018.

[10] C. Liu, "Vortex beam and its application in optical tweezers," in *J. Phys.: Conf. Ser.*, vol. 1549, no. 3, 2020.

[11] J. Yu, C. Zhou, Y. Lu, and J. Wang, "Circular Dammann gratings for enhanced control of the ring profile of perfect optical vortices," *Photonics Res.*, vol. 8, no. 5, pp. 648–658, 2020.

[12] J. Wang, J. Yang, I. M. Fazal, N. Ahmed, and A. E. Willner, "Terabit free-space data transmission employing orbital angular momentum multiplexing," *Nat. Photonics*, vol. 6, no. 7, pp. 488–496, 2012.

[13] S. Fu, T. Wang, S. Zhang, Z. Zhang, and Y. Qin, "Experimental demonstration of free-space multi-state orbital angular momentum shift keying," *Opt. Express*, vol. 27, no. 23, pp. 33111–33119, 2019.

[14] M. Samadzadeh, P. Y. Moghadam, S. Rasouli, and D. Hebri, "Multiplying vortex beams by diffraction from almost periodic structures: Theory and experiment," *Appl. Phys. Lett.*, vol. 124, no. 20, 2024.

[15] D. Hebri and S. Rasouli, "Diffraction from two-dimensional orthogonal nonseparable periodic structures: Talbot distance dependence on the number theoretic properties of the structures," *J. Opt. Soc. Am. A*, vol. 36, no. 2, pp. 253–263, 2019.

[16] P. Y. Moghadam, D. Hebri, S. Rasouli, and M. S. M. Homayoon, "Three-dimensional optical multiple trapping using pure amplitude octagonal almost periodic structures," *Opt. Express*, vol. 31, no. 26, pp. 43490–43505, 2023.

Part Four

Oral presentations

In-Person

Proceedings of the 4th International Conference on Holography and its Applications

18 to 19 September, 2025, Khazar University, Baku, Azerbaijan. ICHA4(2025)401

Full paper - Oral

Confined Position Dependent Mass Harmonic Oscillator as a Model for an Abrupt Semiconductor Heterojunction

Aygun Mammadova
Institute of physics, ministry of science and education of Azerbaijan republic, Azerbaijan
Email: aygun.mammadova@outlook.de

Abstract. Within the position-dependent mass formalism, the Schrödinger equation expressed by the kinetic energy operator for abrupt heterojunctions is exactly solved for harmonic oscillator model and the nonlinear energy spectrum and the wave functions of stationary states are obtained.

The study of effective-mass Hamiltonians for abrupt heterojunctions and the associated wave function matching conditions has been the subject of intense research. We study confined harmonic oscillator model with the Zhu-Kroemer kinetic energy operator as a model of an abrupt heterojunction between two different semiconductors, which has been studied in many investigations. Confinement effect as two infinite high walls at position values $x = \pm a$ is achieved thanks to the effective mass changing with position:

$$M \equiv M(x) = \frac{a^2 m_0}{a^2 - x^2}, \tag{1}$$

The effective mass $M(x)$ varies depending on the coordinate and was proposed by Zhu-Kroemer:

$$\hat{H}_0^{ZK} = -\frac{\hbar^2}{2}\frac{1}{\sqrt{M(x)}}\frac{d^2}{dx^2}\frac{1}{\sqrt{M(x)}} \tag{2}$$

Here V(x) is the potential of the nonrelativistic linear harmonic oscillator under study, defined as:

$$V(x) = \begin{cases} \frac{M(x)\omega^2 x^2}{2}. & -a<x<a \\ \infty. & x=\pm a, \end{cases} \tag{3}$$

and we obtain the following expressions for energy spectrum and the wave functions of the stationary states

$$E \equiv E_n^{ZK} = \hbar\sqrt{\omega^2 + \frac{\hbar^2}{m^2 a^4}}\left(n + \frac{1}{2}\right) + \frac{\hbar^2}{2ma^2}(n^2 + n + 1). \tag{4}$$

$$\psi \equiv \psi_n^{ZK}(x) = c_n^{ZK}\left(1 - \frac{x^2}{a^2}\right)^{\frac{1}{2}\sqrt{\frac{m^2\omega^2 a^4}{\hbar^2}+1}} C_n^{\left(\sqrt{\frac{m^2\omega^2 a^4}{\hbar^2}+1}+\frac{1}{2}\right)}\left(\frac{x}{a}\right). \tag{5}$$

where $C_n^{(\lambda)}(x)$ are Gegenbauer polynomials and c_n^{ZK} is the normalization factor.

From the energy spectrum expression was observed that ground state energy depends on confinement parameter a and angular frequency ω. This case differs it from other known confined oscillator models and was provided probability densities corresponding energy levels aiming to exhibit their behaviour within confinement effect.

References

[1] R.A.Morrow, K.R.Brownstein. Model effective-mass Hamiltonians for abrupt heterojunctions and the associated wave-function-matching conditions, Phys. Rev. B, 30 (1984) 678-680.

[2] M.F.H.Schuurmans, G.W.'t Hooft. Simple calculations of confinement states in a quantum well, Phys. Rev. B, 31 (1985) 8041-8048.

[3] R.A.Morrow. Establishment of an effective-mass Hamiltonian for abrupt heterojunctions, Phys. Rev. B, 35 (1987) 8074-8079.

Talk link: https://youtu.be/IgOW40befd8

Thursday 18th September 2025

Abstract paper – Oral

Vector Meson Gravitational Form Factors and Generalized Parton Distributions within the soft-wall AdS/QCD model

Minaya Allahverdiyeva
Institute of Physics, Baku, Azerbaijan.
The Ministry of Science and Education, Baku, Azerbaijan.
minaallahverdiyeva@ymail.com

Abstract. The accelerating expansion of the universe remains one of the most profound discoveries in modern cosmology, motivating a wide class of dark energy models to explain it. Among these, the holographic dark energy (HDE) model, which is based on the holographic principle of quantum gravity, offers a fascinating framework for explaining cosmic acceleration in the late time. In this paper, we jointly analyze recent cosmological datasets, such as gamma-ray burst (GRB) distance indicators, cosmic chronometer (CC)measurements of the Hubble parameter, and Type Ia supernovae from the Pantheon sample, to present observational constraints on HDE models. We constrain the HDE parameters using Markov Chain Monte Carlo methods and a Bayesian statistical framework. Our findings show that late-time cosmic acceleration can still be explained by HDE models. These findings highlight how crucial holographic methods are for examining the nature of cosmic acceleration and dark energy.

References

[1] Z. Abidin, C. E.Carlson, “Gravitational Form Factors of Vector Mesons in an AdS/QCD Model”, Phys. Rev. D 77, 095007 (2008), [arXiv:hep-th/0801.3839].

[2] X. D. Ji, “Gauge invariant decomposition of nucleon spin”, Phys. Rev. Lett. 78, 610 (1997), [arXiv:hep-ph/9603249].

[3] M. Diehl, “Generalized parton distributions”, Phys. Rept. 388, 41-277 (2003), [arXiv:hep-ph/0307382].

[4] Z. Abidin, C. E.Carlson, “Gravitational Form Factors in the Axial Sector from an AdS/QCD Model”, Phys. Rev. D 77, 115021 (2008), [arXiv:hep-ph/0804.0214].

Talk link: https://youtu.be/IXIoKCiO57k

Thursday 18th September 2025

Full paper – Oral

The exact solution of the hyperbolic pöschl-teller potential by functional method

Shakir M.Nagiyev
Institute of Physics, Ministry of Science and Education, H. Javid Avenue, 131, AZ 1143, Baku, Azerbaijan
Email: shakir.m.nagiyev@gmail.com

Abstract. We obtain by functional method, in exact closed form, both normalized bound state and scattering state wave functions and discrete and continuous spectra for the Schrodinger equation with hyperbolic Pöschl-Teller potential $V = \frac{a}{\sinh^2 \alpha x} - \frac{b}{\cosh^2 \alpha x}$, where $b > a > 0$ and $0 < x < \infty$. These wave functions are derived in terms of the Jacobi polynomials $P_n^{(\alpha,\beta)}(-x)$ with the domain $1 < x < \infty$, $\beta > -1$ and $\alpha + \beta < -2N - 1$. We show that the hyperbolic and the trigonometric Pöschl-Teller potential wells problems are equivalent to the linear singular oscillator models with the position-dependent mass studied in [9].

1 Introduction

In both nonrelativistic and relativistic quantum mechanics, potential models play a key role in studying the physical properties of micro-objects [1-3]. Potential models are based on wave equations, which are the fundamental equations of motion of quantum mechanics. These are the nonrelativistic Schrödinger equation, the relativistic Klein-Gordon equation, the Dirac equation, and the equation of motion of the finite-difference version of relativistic quantum mechanics (see, for example, [4] and the literature therein). There are a variety of well-known physically significant quantum-mechanical potentials. Many of them are phenomenological. For example, the Hulthen potential, the Morse potential, the Rosen-Morse potential, the Kratzer potential, the trigonometric and hyperbolic Pöschl-Teller potentials (see, for example, [1-3]), etc. Many of these interaction potentials have not only many successful applications but also the other important property that they are exactly solvable in the framework of nonrelativistic and relativistic quantum theories (at least in the case $l = 0$).

In [5] Barut et al. used an algebraic method in the one-dimensional case to exactly solve the Schrödinger equation for the Pöschl-Teller hyperbolic potential

$$V_{\mathrm{PT}}(x) = \frac{a}{\sinh^2 \alpha x} - \frac{b}{\cosh^2 \alpha x}, \ 0 < x < \infty \qquad (1)$$

and found both discrete and continuous spectrum, bound state and scattering wavefunctions. Here the parameters a and b are relevant to the potential depth, while real positive parameter α describes the range of the potential. For the special case $a = 0$ was this problem solved before in [1, 6]. In a paper [7]), it was shown that the sl(4, ℝ) Lie algebra has a useful application to the hyperbolic Pöschl-Teller equation.

Hyperbolic Pöschl–Teller potential is an important diatomic molecular potential. This potential has been carried out widely in the quantum physics (see, for example, [8] and Ref.s there).

Our main goal here is to solve exactly one-dimensional Schrödinger equation with hyperbolic Pöschl–Teller potential (1) by a simpler and more direct functional method. In contrast to [5], we find a compact expression for the wave functions of the system under consideration.

On the other hand, it should be noted that central and non-central potential models with coordinate-dependent mass have found wide application in various fields of theoretical physics over the past few decades [9–22]. This is primarily due to the fact that they can, for example, explain well the electronic properties of semiconductors [10, 11], quantum wells, quantum wires and quantum dots [12, 13], the graded alloys and semiconductor heterostructures [10], optical properties of a spherical quantum dot [14,15] and so on.

In this regard, we also note that in a recent paper [9], the authors constructed two exactly solvable semi-infinite and infinite models of a singular one-dimensional quantum oscillator with coordinate-dependent masses within the framework of nonrelativistic quantum mechanics. The first model of a singular oscillator corresponds to the following mass function

$$M(x) = \frac{\nu^2 m_0}{\nu^2 + x^2}, \nu > 0, -\infty < x < \infty, \quad (2)$$

and the second model corresponds to the following mass function

$$M(x) = \frac{\nu^2 m_0}{\nu^2 - x^2}, \nu > 0, 0 < x < \nu. \quad (3)$$

Another goal of our work is to show that the hyperbolic Pöschl–Teller potential well problem is equivalent to the first model, but the trigonometric Pöschl–Teller potential well problem is equivalent to the second model of a linear singular oscillator.

This paper is organized as follows. In Section 2 we обсуждаем физические характеристики the hyperbolic Pöschl-Teller potential well (1). The normalized bound state wave functions and the normalized scattering state wave functions are obtained in this Section. In Section 3 показано, что the hyperbolic Pöschl-Teller potential well problem можно рассматривать как модель сингулярного осциллятора с зависящей от координаты массой $M(x)$ (2). The concluding remarks are given in Section 4. In the Appendix, the equivalence of the trigonometric Pöschl-Teller potential well problem and the model of a singular oscillator with coordinate-dependent mass $M(x)$ (3) is established.

2 Hyperbolic Pöschl–Teller

One starts from the Schrodinger equation with the hyperbolic Pöschl-Teller potential (1)

$$\left(-\frac{\hbar^2}{2m}\partial_x^2 + \frac{a}{\sinh^2 \alpha x} - \frac{b}{\cosh^2 \alpha x}\right)\psi(x) = E\psi(x). \quad (4)$$

Note that equation (4) has both discrete and continuous energy spectra only when

$$b > a > 0. \quad (5)$$

In other cases, we obtain only a continuous spectrum. We will solve equation (4) in case (5). In this regard, we note that the potential (1) has a minimum at

$$x_1 = \frac{1}{2\alpha} \ln \frac{\sqrt[4]{b} + \sqrt[4]{a}}{\sqrt[4]{b} - \sqrt[4]{a}} \quad (6)$$

with value

$$V_{\mathrm{PTmin}} = V_{\mathrm{PT}}(x_1) = -\left(\sqrt{b} - \sqrt{a}\right)^2. \quad (7)$$

This is the depth of the Pöschl-Teller potential well. The function (1) has zero at point

$$x_0 = \frac{1}{2\alpha} \ln \frac{\sqrt{b} + \sqrt{a}}{\sqrt{b} - \sqrt{a}}, (x_0 < x_1). \quad (8)$$

We rewrite the wave function ψ in the form

$$\psi(x) = \sqrt{\cosh\alpha x}\,\Phi(x). \tag{9}$$

By next defining

$$\varepsilon = \frac{2mE}{\hbar^2} + \frac{\alpha^2}{4},\ a' = \frac{2ma}{\hbar^2},\ b' = \frac{2mb}{\hbar^2} + \frac{\alpha^2}{4}, \tag{10}$$

one obtains from the above an equation for Φ:

$$\Phi''(x) + \alpha\tanh\alpha x\,\Phi'(x) + \left(\varepsilon - \frac{a'}{\sinh^2\alpha x} + \frac{b'}{\cosh^2\alpha x}\right)\Phi(x) = 0. \tag{11}$$

Since potential (1) satisfies the following limit relations $\lim_{x\to 0} V_{\mathrm{PT}}(x) = \infty$ and $\lim_{x\to\infty} V_{\mathrm{PT}}(x) = 0$, then for $E < 0$ the energy spectrum will be discrete, and for $E > 0$ will be continuous. Let us consider these cases separately.

2.1. Discrete spectrum. Bound State Solutions

In terms of the variable $t = \sinh^2\alpha x$ $(0 < t < \infty)$ equation (11) takes the form

$$\Phi''(t) + \frac{\tilde{\tau}(t)}{\sigma(t)}\Phi'(t) + \frac{\tilde{\sigma}(t)}{\sigma^2(t)}\Phi(t) = 0, \tag{12}$$

where $\tilde{\tau} = \frac{1}{2} + \frac{3}{2}t,\ \sigma = t(1+t), \tilde{\sigma} = c_2t^2 + c_1t - c_0$ and

$$c_2 = \frac{mE}{2\hbar^2\alpha^2} + \frac{1}{16},$$
$$c_1 = c_2 - c_0 + \frac{mb}{2\hbar^2\alpha^2} + \frac{1}{16},\ c_0 = \frac{ma}{2\hbar^2\alpha^2}. \tag{13}$$

We seek the solution of equation (12) in the form

$$\Phi(t) = \varphi(t)y(t),\ \varphi(t) = t^A(1+t)^B. \tag{14}$$

From the conditions $\lim_{t\to 0}\varphi(t) = 0$ and $\lim_{t\to\infty}\varphi(t) = 0$ (the conditions of square integrability of the wave function) we obtain that $A > 0$ and $A + B < 0$. Therefore, $B < 0$. After some simple calculations for the function $y \equiv y(t)$ (14) we obtain the following equation

$$y''(t) + \frac{\tau(t)}{\sigma(t)}y'(t) + \frac{\bar{\sigma}(t)}{\sigma^2(t)}y(t) = 0,$$
$$\tau(t) = 2A + \frac{1}{2} + \left(2A + 2B + \frac{3}{2}\right)t,\ \bar{\sigma}(t) = \mu_2t^2 + \mu_1t + \mu_0. \tag{15}$$

Here the coefficients μ_2, μ_1 and μ_0 are equal

$$\mu_2 = \mathrm{c}_2 + \frac{1}{2}(A+B) + (A+B)^2,$$
$$\mu_1 = \mathrm{c}_1 + \frac{1}{2}B + 2A(A+B),$$
$$\mu_0 = -\mathrm{c}_0 - \frac{1}{2}A + A^2, \tag{16}$$

and the parameters A and B are arbitrary for now. We will now choose them so that the condition $\bar{\sigma}(t) = \lambda\sigma(t)$, $\lambda = \mathrm{const}$ is satisfied. From this condition we obtain the following equalities

$$\mu_2 = \mu_1 = \lambda,\ \mu_0 = 0. \tag{17}$$

First, from the equality $\mu_0 = 0$ we find the parameter A, and then from the equality $\mu_2 - \mu_1 = 0$ we find the parameter B. We have:

$$A = \frac{1}{4} + \sqrt{\frac{1}{16} + c_0},\ B = -\sqrt{c_0 + \mathrm{c}_1 - \mathrm{c}_2}, \tag{18}$$

or, taking into account (13), we find

$$A = \frac{1}{4} + \sqrt{\frac{1}{16} + \frac{ma}{2\hbar^2\alpha^2}}\,,\ B = -\sqrt{\frac{1}{16} + \frac{mb}{2\hbar^2\alpha^2}}\,. \tag{19}$$

For λ we choose the expression $\lambda = \mu_2 = \mathrm{c}_2 + \frac{1}{2}(A+B) + (A+B)^2$. As a result, for the function $y(t)$ we obtain an equation of hypergeometric type

$$t(1+t)y''(t) + [2A + \frac{1}{2} + \left(2A + 2B + \frac{3}{2}\right)t]y'(t) + \lambda y(t) = 0. \tag{20}$$

Let's find a polynomial solution to this equation in two ways.

a) **First way**. In equation (20) we make a change of variable $t = -z$, i.e. $z = \sinh^2\alpha x$. Then we get

$$z(1-z)y''(-z) + \left[2A + \frac{1}{2} - \left(2A + 2B + \frac{3}{2}\right)z\right]y'(-z) - \lambda y(-z) = 0. \tag{21}$$

Let us now compare equation (21) with the hypergeometric equation [1]

$$z(1-z)u''(z) + [\gamma_1 - (\alpha_1 + \beta_1 + 1)z]\mathrm{u}'(z) - \alpha_1\beta_1 u(z) = 0. \tag{22}$$

The general solution of equation (22) is written as

$$u(z) = \tilde{C}_1\ {}_2F_1(\alpha_1, \beta_1;\ \gamma_1, z) + \tilde{C}_2 z^{1-\gamma_1}\ {}_2F_1(\beta_1 - \gamma_1 - 1, \alpha_1 - \gamma_1 - 1; 2 - \gamma_1, z), \tag{23}$$

where $\gamma_1 \neq 0, -1, -2, \ldots$ Comparison of equations (21) and (22) leads to the equalities

$$\begin{aligned} \alpha_1 &= \tfrac{1}{4} + A + B + \sqrt{K}\,, \\ \beta_1 &= \tfrac{1}{4} + A + B - \sqrt{K}\,, \gamma_1 = 2A + \tfrac{1}{2}, \\ K &= (A + B + \tfrac{1}{4})^2 - \lambda = \frac{1}{16} - \mathrm{c}_2 = -\frac{mE}{2\hbar^2\alpha^2}. \end{aligned} \tag{24}$$

Since $E < 0$, then $K > 0$. In terms of the potential parameters for α_1, β_1 and γ_1 we have the expressions

$$\begin{aligned} \alpha_1 &= \frac{1}{2} + \sqrt{\frac{1}{16} + \frac{ma}{2\hbar^2\alpha^2}} - \sqrt{\frac{1}{16} + \frac{mb}{2\hbar^2\alpha^2}} + \sqrt{-\frac{mE}{2\hbar^2\alpha^2}}\,, \\ \beta_1 &= \frac{1}{2} + \sqrt{\frac{1}{16} + \frac{ma}{2\hbar^2\alpha^2}} - \sqrt{\frac{1}{16} + \frac{mb}{2\hbar^2\alpha^2}} - \sqrt{-\frac{mE}{2\hbar^2\alpha^2}}\,. \\ \gamma_1 &= 1 + \sqrt{\frac{1}{4} + \frac{2ma}{\hbar^2\alpha^2}}. \end{aligned} \tag{25}$$

Since in our case $1 - \gamma_1 < 0$, the second term in (23) diverges at $z = 0$ (or at $x = 0$). Therefore, it must be $\tilde{\mathrm{C}}_2 = 0$. Thus, for the solution of the equation (22) we obtain

$$y(-z) = {}_2F_1(\alpha_1, \beta_1;\ \gamma_1, z) \text{ or}$$

$$y(x) = {}_2F_1(\alpha_1, \beta_1;\ \gamma_1; -\sinh^2\alpha x). \tag{26}$$

In order for the function $y(x)$ to be a polynomial of degree n, we must set

$$\alpha_1 = -n, n = 0, 1, 2, 3, \ldots \tag{27}$$

This is the condition of energy quantization. From this we obtain that the energy levels of the system under consideration are determined by the formula

$$E_n = -\frac{2\hbar^2\alpha^2}{m}\left(n + A + B + \frac{1}{4}\right)^2 = -\frac{2\hbar^2\alpha^2}{m}\left(\sqrt{\frac{1}{16} + \frac{mb}{2\hbar^2\alpha^2}} - \sqrt{\frac{1}{16} + \frac{ma}{2\hbar^2\alpha^2}} - n - \frac{1}{2}\right)^2. \tag{28}$$

There is a finite number of energy levels determined by the condition $\sqrt{K} > 0$, i.e.

$$n < \sqrt{\frac{1}{16} + \frac{mb}{2\hbar^2\alpha^2}} - \sqrt{\frac{1}{16} + \frac{ma}{2\hbar^2\alpha^2}} - \frac{1}{2}. \tag{29}$$

Thus, the desired polynomial solution will have the form

$$y_n(x) = {}_2F_1\left(-n, n+1+\sqrt{\frac{1}{4}+\frac{2mb}{\hbar^2\alpha^2}}-\sqrt{\frac{1}{4}+\frac{2ma}{\hbar^2\alpha^2}};\ 1+\sqrt{\frac{1}{4}+\frac{2ma}{\hbar^2\alpha^2}};-\sinh^2\alpha x\right). \quad (30)$$

Taking into account (9), (14) and (30) we find the wave functions corresponding to the energy levels (28)

$$\psi_n(x) = \tilde{C}_n \sinh^{2A}(\alpha x)\cosh^{2B+1/2}(\alpha x)\ {}_2F_1(-n, n+\tfrac{1}{2}+2A+2B;\ \gamma_1;-\sinh^2\alpha x). \quad (31)$$

Note that condition (29) ensures the square integrability of the wave function: $\int_0^\infty |\psi_n(x)|^2 dx < \infty$.

b) **Second way**. In equation (20) we make a change of variable $t = \frac{\xi-1}{2}$, where $\xi = 1 + 2\sinh^2\alpha x$. Then we get

$$(\xi^2-1)y''(\xi) + \left[2A-2B-\tfrac{1}{2}+\left(2A+2B+\tfrac{3}{2}\right)\xi\right]y'(\xi) + \lambda y(\xi) = 0. \quad (32)$$

Let us compare this equation with the equation for Jacobi polynomials $\bar{y}(x) = P_n^{(\alpha_2,\beta_2)}(-x)$ with the domain $1 < x < \infty$ and $\beta_2 > -1$, $\alpha_2 + \beta_2 < -2N - 1$ [23]

$$(x^2-1)\bar{y}''(x) + [\beta_2 - \alpha_2 + (\alpha_2+\beta_2+2)]\bar{y}'(x) - \lambda_n\bar{y}(x) = 0, \quad (33)$$

where $\lambda_n = n(n+\alpha_2+\beta_2+1)$. In case $1 \le x < \infty$, $\alpha_2 + \beta_2 < -2N - 1$, $\beta_2 > -1$ and $m, n \in \{0, 1, 2, \dots, N\}$ these polynomials satisfy the orthogonality condition of the form

$$\int_1^\infty (x+1)^{\alpha_2}(x-1)^{\beta_2} P_m^{(\alpha_2\,\beta_2)}(-x) P_n^{(\alpha_2\,\beta_2)}(-x)dx =$$

$$= -\frac{2^{\alpha_2+\beta_2+1}}{2n+\alpha_2+\beta_2+1}\frac{\Gamma(-n-\alpha_2-\beta_2)\Gamma(n+\beta_2+1)}{\Gamma(-n-\alpha_2)\,n!}\delta_{mn}, \quad (34)$$

(Note. It should be noted that in formula (9.8.3) of the book [23] (p. 217) there is a typo: instead of $\Gamma(n+\alpha+\beta+1)$ it should be $\Gamma(n+\beta+1)$).

From the comparison of (32) and (33) we find that $\alpha_2 = 2B$, $\beta_2 = 2A - \frac{1}{2}$ and $\lambda = -\lambda_n$. Therefore, $y(\xi) \equiv y_n(\xi) = P_n^{(2B,2A-1/2)}(-\xi)$ or, in terms of x, we have

$$y_n(x) = P_n^{\left(-\sqrt{\frac{1}{4}+\frac{2mb}{\hbar^2\alpha^2}},\sqrt{\frac{1}{4}+\frac{2ma}{\hbar^2\alpha^2}}\right)}(-1-2\sinh^2\alpha x). \quad (35)$$

From the equality $\lambda = -\lambda_n$ it follows for the energy, as it should be, the same formula (28), and from the inequality $\alpha_2 + \beta_2 < -2N - 1$ we obtain the condition $N < -A - B - \frac{1}{4}$, which coincides with the condition (29).

We can now express the wave functions (31) through the Jacobi polynomials

$$\psi_n(x) = C_n \sinh^{2A}(\alpha x)\cosh^{2B+1/2}(\alpha x) P_n^{(2B,2A-1/2)}(-1-2\sinh^2\alpha x), \quad (36)$$

where the parameters A and B are given in (18).

The advantage of writing the wave function in terms of Jacobi polynomials is that using the orthogonality relation (34) we can easily find the normalization constant:

$$C_n = \sqrt{-\frac{2\alpha(2n+2A+2B+1/2)\Gamma(-n-2B)\,n!}{\Gamma(-n-2A-2B+1/2)\Gamma(n+2A+1/2)}}. \quad (37)$$

Let us also present the relationship between the normalization constants $\tilde{C}_n$ and C_n:

$$\tilde{C}_n = C_n \frac{\Gamma(n+2A+1/2)}{\Gamma(2A+1/2)n!}. \quad (38)$$

We emphasize that, taking into account the connection $\kappa_B = 2A$ and $\lambda_B = -2B - 1/2$ between the parameters for the hyperbolic Pöschl-Teller potential (1) of the work of Barut et al [5] and this work, we can verify that the formulas for the energy coincide.

2.2. Continuous spectrum. Scattering State Solutions

The spectrum of positive eigenvalues of the energy for the system under consideration is continuous and extends from zero to infinity. We now turn to solve Eq. (11) for непрерывный спектр. Similarly, we make the same variable $t = \sinh^2 \alpha x$ $(0 < t < \infty)$, define

$$k = \sqrt{2mE}/\hbar,\ q = \frac{1}{4} + A + B = \frac{1}{2} + \sqrt{\frac{1}{16} + \frac{ma}{2\hbar^2\alpha^2}} - \sqrt{\frac{1}{16} + \frac{mb}{2\hbar^2\alpha^2}} < 0. \quad (39)$$

Quantities $\alpha_1,\ \beta_1$ and $\sqrt{K}$, defined by the formula (24), are now complex:

$$\alpha_1 = \frac{1}{4} + A + B + i\,k/(2\alpha),$$
$$\beta_1 = \frac{1}{4} + A + B - i\,k/(2\alpha),$$
$$\sqrt{K} = i\,k/(2\alpha). \quad (40)$$

For the scattering states, $E > 0$ and $k > 0$. As a result, we can get the wave function of the scattering states as

$$\psi(x) = C \sinh^{2A} \alpha x \cosh^{2B+1/2} \alpha x \times$$

$$\times\ {}_2F_1\left(q + i\,k/(2\alpha),\, q - i\,k/(2\alpha);\ 2A + \frac{1}{2}; -\sinh^2 \alpha x\right), \quad (41)$$

where C is a normalization constant. For the wave function (41) we have $\psi(x) \to 0$ при $x \to 0$.

Let us study its asymptotic expression for large x. To this end, using a recurrence relation of the hypergeometric function [1]

$${}_2F_1(\alpha, \beta;\ \gamma; z) = \frac{\Gamma(\gamma)\Gamma(\beta-\alpha)}{\Gamma(\beta)\Gamma(\gamma-\alpha)}(-z)^{-\alpha}\ {}_2F_1(\alpha, \alpha+1-\gamma;\ \alpha+1-\beta; 1/z) +$$
$$+\frac{\Gamma(\gamma)\Gamma(\alpha-\beta)}{\Gamma(\alpha)\Gamma(\gamma-\beta)}(-z)^{-\beta}\ {}_2F_1(\beta, \beta+1-\gamma;\ \beta+1-\alpha; 1/z) \quad (42)$$

and ${}_2F_1(\alpha, \beta;\ \gamma; 0) = 1$, we have

$${}_2F_1(\alpha_1, \beta_1;\ \gamma_1; -\sinh^2 \alpha x) \underset{x\to\infty}{\longrightarrow} \Gamma(\gamma_1) e^{-2q\alpha x}(De^{-ikx} + D^* e^{ikx}), \quad (43)$$

where

$$D = \frac{1}{4}\frac{\Gamma(\beta_1-\alpha_1)}{\Gamma(\beta_1)\Gamma(\gamma_1-\alpha_1)} = \frac{1}{4}\frac{\Gamma(-ik/\alpha)}{\Gamma(q-ik/2\alpha)\Gamma(\gamma_1-q-ik/2\alpha)}. \quad (44)$$

By setting $D = |D|e^{-i\delta}$ we have

$${}_2F_1(\alpha_1, \beta_1;\ \gamma_1; -\sinh^2 \alpha x) \underset{x\to\infty}{\longrightarrow} 2\,|D|\Gamma(\gamma_1) e^{-2q\alpha x} \cos(kx + \delta). \quad (45)$$

Substituting this formula into Eq. (39), we finally obtain

$$\psi(x) \equiv \psi_k(x) \underset{x\to\infty}{\longrightarrow} \frac{1}{2} C|D|\Gamma(\gamma_1) \cos(kx + \delta). \quad (46)$$

By comparing this formula with the general boundary condition of the wavefuntions normalized by the delta function of p (the momentum of the particle at infinity) [1] $\psi_p(x) \approx \sqrt{2/\pi\hbar}\cos(kx+\delta)$, we obtain the normalization constant as follows

$$C = 8\sqrt{2/\pi\hbar}\,\frac{1}{\Gamma(2A+1/2)}\left|\frac{\Gamma(A+B+1/4-ik/2\alpha)\Gamma(A-B+1/4-ik/2\alpha)}{\Gamma(-ik/\alpha)}\right|. \quad (47)$$

At the end of this section we note that according to (43) we obtain the reflection and transmission coefficients as $R = 1$ and $T = 0$, i.e. due to the infinite potential wall at the point $x = 0$ the particle is completely reflected from the wall.

3 Hyperbolic Pöschl-Teller potential well as a model of the singular oscillator with position-dependent mass

In this section we will show that the hyperbolic Pöschl-Teller potential well (4) can be considered as a model of a singular oscillator with coordinate-dependent mass $M(x)$ (2), proposed in [9]. To do this, it is sufficient to verify that the Schrödinger equations describing these models coincide in form after some transformations. For example, we transform the Schrödinger equation

$$[\partial_x^2 - \frac{M'}{M}\partial_x + \frac{2M}{\hbar^2}(E-V)]\psi(x) = 0 \quad (48)$$

for the model of a singular oscillator with mass $M(x)$ (2) and potential

$$V = \frac{M(x)\omega^2x^2}{2} + \frac{g}{x^2} = \frac{m_0\nu^2\omega^2x^2}{2(\nu^2+x^2)} + \frac{g}{x^2},\ 0 < x < \infty \quad (49)$$

to the form (11). This is easy to do if we pass to a new variable $x = \nu\sinh\alpha t$. Then we obtain an equation that coincides in form with (11)

$$\psi''(t) + \alpha\tanh\alpha t\psi'(t) + \left(\varepsilon_1 - \frac{a_1'}{\sinh^2\alpha t} + \frac{b_1'}{\cosh^2\alpha t}\right)\psi(t) = 0. \quad (50)$$

Here the following quantities are analogous to (10)

$$\varepsilon_1 = \frac{2m_0\alpha^2\nu^2}{\hbar^2}E - b_1',\ a_1' = \frac{2m_0\alpha^2 g}{\hbar^2},\ b_1' = \frac{m_0^2\alpha^2\omega^2\nu^4}{\hbar^2}. \quad (51)$$

The analogues of the parameters (18) will be

$$A_1 = \frac{1}{4} + \sqrt{\frac{1}{16} + \frac{a_1'}{4\alpha^2}} = \frac{1}{4} + \frac{d}{2},\ ,\ B_1 = -\frac{1}{2\alpha}\sqrt{b_1'} = -\frac{1}{2}\lambda_0^2\nu^2,$$

$$d = \frac{1}{2}\sqrt{1 + \frac{8m_0g}{\hbar^2}},\ \ \lambda_0 = \sqrt{\frac{m_0\omega}{\hbar}}. \quad (52)$$

Using this analogy we can find the energy spectrum and the wave function for the singular oscillator model (48). As an example, we derive from formulas (28), (51) and (52) the discrete energy spectrum (1) of [9]. We easily obtain that

$$E_n^{\mathrm{so}} = \frac{2\hbar^2}{m_0\nu^2}\left[\frac{1}{16} - \left(n + A_1 + B_1 + \frac{1}{4}\right)^2\right] + \frac{m_0\omega^2\nu^2}{2}, n < -A_1 - B_1 - \frac{1}{4}, \quad (53)$$

or

$$E_n^{so} = \frac{\hbar^2}{2m_0\nu^2}\left[\frac{1}{4} - (2n + d + 1 - \lambda_0^2\nu^2)^2\right] + \frac{m_0\omega^2\nu^2}{2}, n < \frac{1}{2}(\lambda_0^2\nu^2 - d - 1). \quad (54)$$

In the same way, we can easily find the explicit form of the wave function of the singular oscillator model.

4 Conclusions

We obtained exactly both bound state and scattering state solutions to the Schrödinger equation with the hyperbolic Pöschl–Teller potential. In this case, we used the functional method. It is shown that the solutions can be expressed by the hypergeometric functions ${}_2F_1(\alpha, \beta; \gamma; z)$. We also expressed the bound state wawe functions through Jacobi polynomials $P_n^{(\alpha,\beta)}(-x)$, where $x > 1$. We have shown that the hyperbolic Pöschl-Teller potential well can be regarded as the potential of a singular oscillator with coordinate-dependent mass $M(x) = \frac{\nu^2 m_0}{\nu^2 + x^2}$, $\nu > 0$. Both of these potentials admit of a finite number of bound states.

In this connection, we note that other well-known exactly solvable quantum mechanical models can also be interpreted as new quantum mechanical systems with coordinate-dependent mass. For example, in [24] it was shown that the exact solution of the angular part of the Schrödinger equation with one of the Hautot potentials corresponds to an exactly solvable model of a linear harmonic oscillator with coordinate-dependent mass in a homogeneous gravitational field. Another example is given in the Appendix.

Appendix

In [9] we have developed a second exactly solvable model of a linear singular harmonic oscillator with mass dependent on the coordinates (3). This model corresponds to the potential

$$V = \frac{M(x)\omega^2 x^2}{2} + \frac{g}{x^2} \equiv \frac{m_0\nu^2\omega^2 x^2}{2(\nu^2 - x^2)} + \frac{g}{x^2}, \ 0 \le x \le \nu. \quad (A.1)$$

The Schrödinger equation for model (A.1) is written as

$$(\nu^2 - x^2)\frac{d^2\psi}{dx^2} - 2x\frac{d\psi}{dx} + \left(\frac{2m_0\nu^2 E}{\hbar^2} - \frac{2m_0\nu^2 g}{\hbar^2 x^2} - \frac{{\lambda_0}^4\nu^4 x^2}{\nu^2 - x^2}\right)\psi = 0. \quad (A.2)$$

We show that this model (A.1) can be interpreted as a trigonometric Pöschl-Teller potential well. The trigonometric Pöschl-Teller equation is

$$\left\{-\frac{\hbar^2}{2m_0}\frac{d^2}{dx^2} + \frac{1}{2}V_0\left[\frac{\kappa(\kappa-1)}{\sin^2\alpha x} + \frac{\lambda(\lambda-1)}{\cos^2\alpha x}\right]\right\}\psi = E\psi. \quad (A.3)$$

Here, $\kappa > 1$, $\lambda > 1$ and the notation $V_0 = \frac{\hbar^2\alpha^2}{m_0}$ is introduced for simplicity. In the region $0 \le x \le \frac{\pi}{2\alpha}$, where the potential becomes infinitely high at the borders of this region, the wavefunction has to possess the following boundary condition:

$$\psi(0) = \psi\left(\frac{\pi}{2\alpha}\right) = 0. \quad (A.4)$$

The solution to equation (A.3) was found in [3, 25].

In equation (A.2) we make a change of variable$x = \nu \sin \alpha z$, where now the condition $0 \leq z \leq \frac{\pi}{2\alpha}$ holds. Then, one obtains that

$$\left[\frac{d^2}{dz^2} - \alpha \tan \alpha z \frac{d}{dz} + \alpha^2 \left(c_0 + c_2 - \frac{c_1}{\sin^2 \alpha z} - \frac{c_2}{\cos^2 \alpha z}\right)\right] \psi = 0, \tag{A.5}$$

where $c_0 = \frac{2m_0 \nu^2 E}{\hbar^2}$, $c_1 = \frac{2m_0 g}{\hbar^2}$, $c_2 = \lambda_0^4 \nu^4$. Then, we look for the solution of (A.5) as

$$\psi = \frac{1}{\sqrt{\cos \alpha z}} \cdot \Phi(z). \tag{A.6}$$

Now, one observes that equation for $\Phi(z)$ coincides with equation (A.3)

$$\left[\frac{d^2}{dz^2} + \alpha^2 \left(c_0 + c_2 + \frac{1}{4}\right) - \alpha^2 \left(\frac{c_1}{\sin^2 \alpha z} + \frac{c_2 + \frac{1}{4}}{\cos^2 \alpha z}\right)\right] \Phi(z) = 0. \tag{A.7}$$

The wave function $\Phi(z)$ also satisfies a boundary condition of the form (A.4).

Thus, we have shown that a singular harmonic oscillator with coordinate-dependent mass (A.2) and the trigonometric Pöschl-Teller potential well problem (A.3) are directly connected through the elegant mathematical transform.

References

[1] L.D. Landau and E.M. Lifshitz, Quantum Mechanics 3rd edn. (Pergamon Press, 1979).

[2] W. Greiner, Relativistic Quantum Mechanics, 3rd edn. (Springer, 2000).

[3] S. Flügge, Practical Quantum Mechanics, Vol. 1 (Springer, 1994).

[4] Sh.M. Nagiyev, E.I. Jafarov and R.M. Imanov, The relativistic linear singular oscillator , J. Phys. A: Math. Gen. 36 (2003) 7813–7824.

[5] A.O. Barut, A. Inomata and R. Wilson, Algebraic treatment of second Pöschl-Teller, Morse-Rosen and Eckart equations, J. Phys. A: Math. Gen. 20 (1987) 4083-4096.

[6] M.M. Nieto, Exact wave-function normalization constants for the B_0 tanhz- U_0 〖cosh〗^(-2) z and Pöschl-Teller potentials, Phys. Rev. A 17 (1978) 1273-1283.

[7] C. Quesne, An sl(4, R) Lie algebraic approach to the Bargmann functions and its application to the second Pöschl-Teller equation, J. Phys. A: Math. Gen. 22 (1989) 3723-3730.

[8] Y. You, F. L. Lu, D. S. Sun, C. Y. Chen, S.H. Dong, Solutions of the second Pöschl-Teller potential solved by an improved scheme to the centrifugal term, Few-Body Syst 54 (2013) 2125-2132.

[9] E.I. Jafarov and Sh.M. Nagiyev, Quantum singular oscillator with potential controlled by position-dependent mass, Turkish J. Phys. 48 (2024) 153 – 178.

[10] G. Bastard, Wave Mechanics Applied to Semiconductor Heterostructure (Les Editions de Physique, 1988).

[11] C. Weisbuch and B. Vinter, Quantum Semiconductor Heterostructures (Academic, New York, 1997).

[12] P. Harrison, Quantum Wells, Wires and Dots (John Wiley and Sons, 2000).

[13] P. Harrison, A. Valavanis, Quantum Wells, Wires and Dots: Theoretical and Computational Physics of Semiconductor Nanostructures (Wiley, Chichester, 2016).

[14] A. Keshavarz and N. Zamani, Optical properties of spherical quantum dot with position-dependent effective mass, Superlat. Microstruct. 58 (2013) 191–197.

[15] R.M. Lima and H.R. Christiansen, Energy eigenstates of position-dependent mass particles in a spherical quantum dot, Eur. Phys. J. B 96 (2023) 150.

[16] A. de Souza Dutra and C.A.S. Almeida, Exact solvability of potentials with spatially dependent effective masses, Phys. Lett. A 275 (2000) 25-30.

[17] S.H. Dong, J.J. Pena, C.P. Garcia and J.G. Ravelo, Algebraic approach to the position-dependent mass Schrödinger equation for a singular oscillator, Mod. Phys. Lett. A, 22 (2007) 1039-1045.

[18] C. Quesne, Point canonical transformation versus deformed shape invariance for position-dependent mass. SIGMA 5, 046 (2009).

[19] C. Quesne, Comment on ’Exact solution of the position-dependent effective mass and angular frequency Schrödinger equation: harmonic oscillator model with quantized confinement parameter’. J. Phys. A: Math. Theor. 54, 368001 (2021).

[20] C. Quesne, Generalized semiconfined harmonic oscillator model with a position-dependent effective mass. Eur. Phys. J. Plus 137, 225 (2022).

[21] E.I. Jafarov, S.M. Nagiyev and A.M. Jafarova, Quantum-mechanical explicit solution for the confined harmonic oscillator model with the von Roos kinetic energy operator. Rep. Math. Phys. 86, 25 (2020) 12.

[22] E.I. Jafarov, S.M. Nagiyev, R. Oste and J. Van der Jeugt, Exact solution of the position-dependent effective mass and angular frequency Schrödinger equation: harmonic oscillator model with quantized confinement parameter. J. Phys. A: Math. Theor. 53, 485301 (2020).

[23] R. Koekoek, P.A. Lesky and R.F. Swarttouw, Hypergeometric orthogonal polynomials and their q - analogues, Springer Verslag, Berlin 2010.

[24] E. I. Jafarov, S. M. Nagiyev, Angular part of the Schrödinger equation for the Hautot potential as a harmonic oscillator with position-dependent mass in a uniform gravitational field, Theor. and Math. Phys., 207(1): 447–458 (2021).

[25] A.O. Barut, A. Inomata, R. Wilson, A new realization of dynamical groups and factorization method, J. Phys. A: Math. Gen. 20 (1987) 4075-4082.

Talk link: https://youtu.be/zhuaLfmP4cI

Thursday 18th September 2025

Full paper – Oral

Electromagnetic radii for the $N + \gamma^* \rightarrow N^*(1440, 1710, 1535)$ transition in holographic model

Sh.I.Taghiyeva[1] and Sh.A.Mamedov[2]
[1]Shamakhy Astrophysical Observatory, Ministry of Science and Education, Theoretical Physics Department, Azerbaijan
Email: shahnazilgarzade@gmail.com
[2]Physics Faculty, Baku State University, Baku, Azerbaijan
Email: shmamedov62@gmail.com

Abstract. It is known that hadrons, including nucleons and their excited states, are not pointlike particles and have their own internal structure. Electromagnetic interaction plays an important role in studying the internal structure of nucleons. Because the form factors in elastic and inelastic scatterings and the determination of these structure functions in deep inelastic scattering of electrons are a rich source of information for studying the structure of the nucleon.

After determining the electromagnetic form factors $F_{1,2}(Q^2)$ for the nucleon-excited nucleon transition, we can determine the electric and magnetic Sachs form factors, which are alternative Lorentz invariant quantities for the proton and neutron constituting the nucleon for the $N + \gamma^* \rightarrow N^*(1440, 1710, 1535)$ transitions. Using these form factors, the charge and magnetic radii of the nucleon are determined framework hard wall AdS/QCD model as follows:

$$r_{E,M}^2 = -6 \frac{dG_{E,M}(Q^2)}{dQ^2}\bigg|_{Q^2=0}$$

We have shown the differences between our results and experimental data for the unexcited nucleons are small and compared with the data [2]. Also, the comparison of soft-wall model results with the ground state nucleons shows on small differences between them. This allows us to make conclusion that the radii have a little change on excitation.

References

[1] G. Ramalho, “Analytic parametrization of the N+γ^*→N^*(1440) form factors inspired by light-front holography”, Phys. Rev. D 96(5), 054021(2017)

[2] K. Nakamura, Review of particle physics. J.Phys. G:Nucl.Particle Phys. 37, 7 (2020)

Talk link: https://youtu.be/y4PRiwG5-OQ

Thursday 18th September 2025

Abstract paper – Oral

Particle and Antiparticle in DSR theories: Nonrelativistic limits of the Dirac equations

Nosratollah Jafari Sonbolabadi
Center for Theoretical Physics, Khazar University, 41 Mehseti Street, Baku, AZ1096, Azerbaijan
nosrat.jafari@gmail.com

Abstract. We study the nonrelativistic limits of the DSR theories. By investigating the nonrelativistic limits of the corresponding Dirac equations in DSR, we study the particle and the antiparticle in these theories. The difference between particle's and the antiparticle's mass is proportional to mc^2/E_p in the first order of approximation. (E_p is the Planck energy) These different masses lead to the violation of CPT invariance. We use this ratio to find an upper limit on the photon mass. Also, we will obtain a lower bound on the amount of E_p. Furthermore, we will discuss the consequences of these effects for the new physics beyond the standard model and quantum gravity.

References

[1] J. Magueijo, L. Smolin, Phys. Rev. Lett., 88 (2002), Article 190403

[2] G. Amelino-Camelia, Int. J. Mod. Phys. D, 11 (2002), p. 35

[3] G. Amelino-Camelia, Int. J. Mod. Phys. D, 11 (2002), p. 1643

[4] Kazuo Fujikawa, Anca Tureanu, Int.J.Mod.Phys.A 32 (2017) 09, 1741014

[5] Nosratollah Jafari and Bekdaulet Shukirgaliyev ,Phys.Lett.B 853 (2024) 138693,

[6] M. Coraddu, S. Mignemi, Europhys. Lett., 91 (2010), Article 51002

[7] N.R. Bruno, G. Amelino-Camelia, J. Kowalski-Glikman, Phys. Lett. B, 522 (2001), p. 133

[8] P. Gosselin, A. Berard, H. Mohrbach, S. Ghosh, Phys. Lett. B, 660 (2008), p. 267

[9] Z. Belhadi, F. Menas, A. Berard, P. Gosselin, H. Mohrbach, Int. J. Mod. Phys. A, 27 (2012), Article 1250031

[10] E. Harikumar, M. Sivakumar, Mod. Phys. Lett. A, 26 (2011), p. 1103

[11] S.A. Franchino-Viñas, J.J. Relancio, Class. Quantum Gravity, 40 (2023), Article 054001

[12] K.A. Olive, et al., Particle Data Group, Chin. Phys. C, 38 (2014), Article 090001

[13] A.D. Dolgov, EPJ Web Conf., 95 (2015), Article 03007

[14] N. Jafari, M.R.R. Good, Phys. Lett. B, 135735 (2020)

Talk link: https://youtu.be/EKwUhih7_is

Thursday 18th September 2025